Symmetry and Broken-Symmetry in Molecular Orbital Descriptions of Unstable Molecules. 3. The Nature of Chemical Bonds of Spin Frustrated Systems[†]

T. Kawakami,*[,‡] R. Takeda,[‡] S. Nishihara,[‡] T. Saito,[‡] M. Shoji,[‡] S. Yamada,[‡] S. Yamanaka,[⊥] Y. Kitagawa,[‡] M. Okumura,[‡] and K. Yamaguchi[§]

Department of Chemistry, Graduate School of Science, Osaka University, 1-1 Machikaneyama, Toyonaka, Osaka 560-0043, Japan, Nanomaterial Design Center, Osaka University, 1-1 Machikaneyama, Toyonaka, Osaka 560-0043, Japan, and Institute for Protein Research, Osaka University, Suita, Osaka 565-0871, Japan

Received: June 26, 2009; Revised Manuscript Received: October 15, 2009

Symmetry and broken symmetry in the molecular orbital description of spin frustration systems have been investigated in relation to the resonating valence bond (RVB) theory of the spin liquid state and non-BCS superconductivity. Broken symmetry (BS) and resonating BS (RBS) molecular orbital (MO) methods have been employed to obtain resonating valence bond (RVB)-type explanations of spin frustrated systems. RBS MO solutions are expanded using the localized molecular orbitals (LMO) to elucidate a universal MO−VB description. The BS and RBS MO descriptions of triangular spin frustrated systems corresponding to transition structures for exchange-forbidden radical insertions were investigated in comparison with the RVB-type explanations of such systems. The BS and RBS calculations by the use of three different axial (SDW) solutions or three noncollinear GSO (helical SDW) solutions of a triangular hydrogen cluster were performed to obtain potential curves with and without resonance (quantum) effects. The resonating GSO (noncollinear) state responsible for short-range correlation was found to be the most stable for the system. The reliability of the approximate spin projection (AP) procedure to eliminate the high-spin component was also elucidated, comparing with the AP BS and RBS potential curves. The BS GSO (GHF) computations of several triangular systems, $N(CH_2)_3$, $(CH_2)_3$, and $Mn(II)_3O_4$, were performed to obtain total energies and total spin angular momentums and effective exchange integrals (J) between local spins, which are crucial for construction of effective spin Hamiltonian models. The exact diagonalization of the Heisenberg models was also performed to depict the energy levels and magnetic susceptibility curves for triangular and kagome lattices to elucidate spin frustration effects and related quantum spin behaviors. Implications of the computational results have been discussed in relation to magnetic properties of several triangular and kagome systems synthesized recently and the superconductivity of triangular systems discovered recently.

I. Introduction

Chemical bonds in molecules and molecular clusters have been described with molecular orbital (MO) and valence bond (VB) methods. The MO theory is now well-accepted for the purpose because one-electron orbital picture based on an independent particle model is simple and lucid. However, the VB theory directly related to electron pairing (two electron picture) has been accepted for renewed interest for several reasons. For example, spin frustrated systems have been receiving continuous theoretical and experimental interest in relation to fundamental theories of quantum spin, spin liquid state, and high-T_c superconductivity.[1−29] Anderson[8,9] already examined electronic states of triangular systems and proposed the resonating valence bond (VB) state, which is written with resonance of three VB configurations as illustrated in Scheme 1. These VB configurations are written using three site orbitals a, b, and c,[30−32] where an unpaired electron remains at different sites for different VB configurations, indicating spin frustration.[10,11]

$$\mathrm{VB(ab)} = \left|\frac{1}{\sqrt{2}}(a\bar{b} + \bar{a}b)c\right| = \left|\frac{1}{\sqrt{2}}(\mathbf{I} - \mathbf{II})\right| = \mathrm{DS(ab)} \tag{1a}$$

$$\mathrm{VB(ca)} = \left|\frac{1}{\sqrt{2}}(c\bar{a} + a\bar{c})b\right| = \left|\frac{1}{\sqrt{2}}(\mathbf{II} - \mathbf{III})\right| = \mathrm{DS(ca)} \tag{1b}$$

$$\mathrm{VB(cb)} = \left|\frac{1}{\sqrt{2}}(c\bar{b} + \bar{c}b)a\right| = \left|\frac{1}{\sqrt{2}}(\mathbf{III} - \mathbf{I})\right| = \mathrm{DS(cb)} \tag{1c}$$

The spin frustration is often explained with three classical expressions of spins as shown in Scheme 2.[33,34]

$$\mathbf{I} = |a\bar{b}c| \qquad \mathbf{I} = |\bar{a}bc| \qquad \text{and} \qquad \mathbf{III} = |ab\bar{c}| \tag{2}$$

The up and down axial vectors mean the up and down spins of electrons, respectively, in conformity with conventional expressions used in chemistry. In this notation, spin-parallel sites exist in each configuration, leading to a classical expression of spin frustration. The three doublet configurations are expressed with out of phase combinations of the classical structures as shown

[†] Part of the "Vincenzo Aquilanti Festschrift".
* To whom correspondence should be addressed.
[‡] Graduate School of Science.
[⊥] Institute for Protein Research.
[§] Nanomaterial Design Center.

10.1021/jp905991r
Published on Web 11/12/2009

SCHEME 1

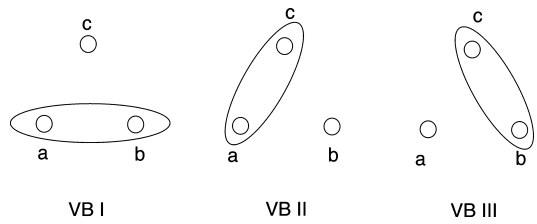

SCHEME 2

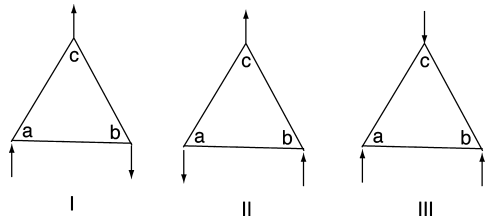

in eq 1.[35] Each configuration is expressed with doublet plus local singlet pairs DS(de), a singlet pair between d and e sites (d, e = a, b, c). However, three VB configurations in eq 1 are overcomplete because there are only two independent total doublet wave functions for three-spin systems with $S_z = 1/2$.[31]

The other doublet wave function corresponding to each local singlet one is expressed with spin coupling between a local triplet configuration and doublet configuration as

$$\mathrm{DT(ab)} = \frac{1}{\sqrt{6}}\{2\mathbf{III} - (\mathbf{I} + \mathbf{II})\} \tag{3a}$$

$$\mathrm{DT(ca)} = \frac{1}{\sqrt{6}}\{2\mathbf{I} - (\mathbf{II} + \mathbf{III})\} \tag{3b}$$

$$\mathrm{DT(cb)} = \frac{1}{\sqrt{6}}\{2\mathbf{II} - (\mathbf{III} + \mathbf{I})\} \tag{3c}$$

The total doublet state with local triplet configuration DT(ab) is regarded as the superposed state of local singlet pairs, VBII(ca) and VBIII(cb), namely, c−a and c−b covalent bonds.[35] On the other hand, the total quartet (QT) wave functions ($S = 3/2$) with a local triplet pair are given by[31]

$$\mathrm{QT(ab)} = \frac{1}{\sqrt{3}}\{\mathbf{III} + (\mathbf{I} + \mathbf{II})\} \tag{4a}$$

$$\mathrm{QT(ca)} = \frac{1}{\sqrt{3}}\{\mathbf{I} + (\mathbf{II} + \mathbf{III})\} \tag{4b}$$

$$\mathrm{QT(cb)} = \frac{1}{\sqrt{3}}\{\mathbf{II} + (\mathbf{III} + \mathbf{I})\} \tag{4c}$$

for which the electron pair bond is broken. Thus 3 × 3 configuration interactions (CI) using three VB configurations in eq 1 or three classical configurations in eq 2 provide two independent doublets and one quartet in eqs 1, 3, and 4.

Chemically, the triangle configuration has been introduced as a transition state of the insertion reaction of the free radical into a covalent bond, as illustrated in Scheme 3.[35]

SCHEME 3

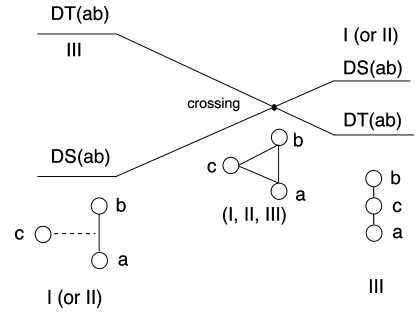

SCHEME 4

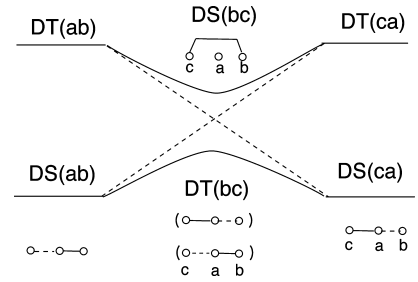

The DS(ab) and DT(ab) states with different permutation symmetry are degenerate in energy at the triangle transition state (TS), indicating the curve crossing between two doublet surfaces. The correlation diagram of the spin vector model also indicates the sudden change of spin structure characterized with the magnetic group,[33,34] **I** (or **II**) → (**I**, **II**, **III**) → **III** at the TS. Then, the insertion reaction with the free radical is regarded as exchange, permutation, or spin-symmetry-forbidden.

On the other hand, such curve crossing does not occur along with the abstraction pathway of the free radical, as shown in Scheme 4. The doublet wave function DS(ab) mixes with the other doublet DT(ab), which is the so-called spin polarization (SP) configuration, in the course of the abstraction reaction, affording the doublet state responsible for the abstraction reaction product, c + ab → ca + b.[36−38] The classical spin structure **II** is also retained throughout the reaction. Therefore, the abstraction reaction with the free radical is characterized as exchange, permutation, or spin-symmetry-allowed. These selection rules for free radical reactions[33−35] are wholly compatible with accumulated experimental results. Potential curves for abstraction and insertion reactions with the free radical have been calculated using the semiempirical VB methods on the basis of the assumption that site orbitals a, b, and c are atomic orbitals (AO).[36−38] However, the VB-type computations are not easy if site orbitals are more or less delocalized over polyatomic molecules.[39]

Molecular orbital (MO)-type computations are rather easy, even for complex radical systems. Configuration correlation diagrams based on the classical vector models in eq 2 are useful for elucidation of characteristic differences between insertion and abstraction reactions with the free radical, as shown in Schemes 3 and 4. This implies that electronic mechanisms of free radical reactions can be easily investigated with the broken symmetry (BS) method under the single determinant constraint (see eq 2) since site orbitals (a, b, and c) in eq 2 are replaced with BS MOs which are more or less delocalized over reacting molecular systems.[40−42] The past decade's BS MO method based on the hybrid Kohn−Sham DFT has been successfully applied for locations of transition structures of oxygenation reactions via radical pathways.[43−60] For example, the compound I (CpdI)

consisting of the iron−oxo Fe(IV)═O and ligand radical (•L) parts was essentially regarded as three-spin systems. Mechanisms of hydrogen abstraction reactions with CpdI have indeed been grasped with BS MOs determined with HDFT calculations. However, 3 × 3 BS MO CI by the use of three BS configurations, **I**−**III**, with BS MOs are inevitable for separation of doublet and quartet states, namely, elimination of quartet spin contamination involved in the BS HDFT solutions.[60] An approximate spin projection (AP) for BS MO solutions has also been performed as a practical procedure for the purpose.[60]

The above examples clearly indicate that triangular systems with spin frustration are very important and interesting in relation to basic notions in condensed matter physics[1−29] and theory of radical reactions.[30−60] However, theoretical studies of such systems are still limited in quantum chemistry. In this paper, electronic structures of several triangular systems are investigated on the basis of the broken symmetry (BS) methods which permit both axial (ASDW) and helical (HSDW) spin density wave (SDW) solutions; note that ASDW and HSDW provide one- and two-dimensional spin densities, respectively.[61−63] The 3 × 3 BS MO CI by the use of three BS solutions is also performed to elucidate the resonance effect in triangular systems with spin frustration, $N(CH_2)_3$, $(CH_2)_3$, and $Mn(II)_3O_4$.[63] To this end, BS MOs are expanded using localized molecular orbitals (LMO) to clarify resonating valence bond (RVB) concepts via LMO CI treatment. Implications of present computational results are also discussed in relation to molecular design of spin frustrated systems[63] and exotic magnetic behaviors observed for mesoscopic clusters with triangle and kagome spin lattices. Finally bottom-up syntheses of spin frustrated systems with physical methods developed in the field of physical chemistry are pointed out.

II. Theoretical Backgrounds

II.1. Universal MO−VB Theory for Chemical Bonds. Theoretical backgrounds for a universal MO−VB description of chemical bonds are briefly introduced in this section. Chemical bonds in molecules have been understood with molecular orbital (MO)[64,65] and valence bond[30−32] theories. Transformations from MO to VB (vice versa) descriptions of chemical bonds have also been performed in several manners. We have proposed a universal MO−VB approach[66] based on symmetry and broken symmetry properties of one-electron orbitals obtained with Hartree−Fock (HF)[67,68] and Kohn−Sham (KS) density functional theory (DFT) under the single determinant approximation (constraint).[69] The HF and KS DFT methods are nonlinear equations in contrast to Hückel MO (HMO) theory, and therefore, these methods combined with variational (self-consistent field (SCF)) principles permit broken symmetry (BS) orbitals under the condition that the covalent bonding interaction (β) becomes weak as compared with the electron−electron repulsion interaction (U); this condition is mathematically formulated as the instability condition.[70] This characteristic change of the one-electron orbital based on the independent particle models is not a real phase transition because molecules under consideration belong to a finite quantum system.[66] However, such a pseudo-phase transition of the molecular orbital may be regarded as a continuous but rapid change of the nature of the chemical bond, namely, its chemical correspondence is changed from the nonradical state to the diradical and/or polyradical one.[61−63,70]

Extraction of radical orbitals among a lot of spin-polarized (SP) molecular orbitals (MO) is often necessary for construction

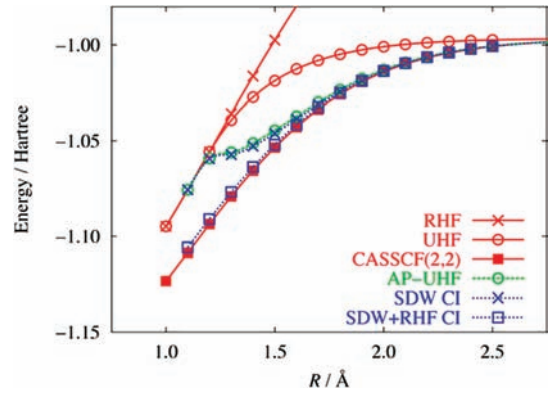

Figure 1. Potential curves of the hydrogen molecule calculated with RHF, UHF, CASSCF[2,2], AP UHF, SDW-CI (resonating BS(RBS)), and SDW+RHF CI methods. The computational results are wholly compatible with theoretical formulations and the Hubbard model. The CI mixing of the RHF solution improves the cusp on the RBS(+) curve because of partial elimination of ionic terms (dynamical correlation).

of lucid orbital interaction schemes for unstable molecules. The natural orbital analysis of BS HF and KS DFT solutions provides two strongly correlated natural molecular orbitals (NMO) and their occupation numbers, which are closely related to diradical electrons in molecules. Here, these symmetry-adapted NMOs are referred to as the highest occupied NO (HONO) and the lowest unoccupied NO (LUNO); note that other occupied orbitals are essentially closed-shell type in the case of diradicals. The localized molecular orbitals (LMOs) at sites a and b are defined with complete mixing of HONO and LUNO as

$$\phi_a = \frac{1}{\sqrt{2}}(\phi_{HONO} + \phi_{LUNO})$$
$$\phi_b = \frac{1}{\sqrt{2}}(\phi_{HONO} - \phi_{LUNO}) \quad (5a)$$

where LMOs are orthogonal and broken symmetry if HONO and LUNO have different spatial symmetries. The BS MOs for diradicals are more or less delocalized and therefore are given with mixing site orbitals

$$\psi^{+}_{HO} = \cos\omega\phi_a + \sin\omega\phi_b \quad (5b)$$

$$\psi^{-}_{HO} = \cos\omega\phi_b + \sin\omega\phi_a \quad (5c)$$

where ω is the orbital mixing parameter. The BS MOs reduce to the closed-shell molecular orbital $\psi^{+}_{HO} = \psi^{-}_{HO} = \phi_{HO}$ the for nonradical state at the triplet instability threshold ($\omega = \pi/4$).[66−70] On the other hand, these are equivalent to site orbitals (LMOs) at the strong correlation limit, $\psi^{+}_{HO} = \phi_a$ and $\psi^{-}_{HO} = \phi_b$ at $\omega = 0$.[71,72] Thus, BS MOs are variable from the MO limit to the VB limit, indicating a universal MO−VB character depending on the strength of the covalent bonding parameter ($x = \beta/U = -t/U$).[66] It is, however, noteworthy that ϕ_a and ϕ_b are localized but orthogonal molecular orbitals (LMO) instead of nonorthogonal atomic orbitals in the Heitler−London theory.[30]

It is interesting and important to elucidate interrelationships between BS MOs and VB functions because of renewed interest in the VB concept.[40−43] To this end, the BS solution given by a single determinant consisting of BS MOs is expanded using LMOs as follows

$$|\mathrm{BSI}\rangle = |\psi^{+}_{\mathrm{HO}}\overline{\psi^{-}_{\mathrm{HO}}}| \tag{6a}$$

$$\begin{aligned}
&= |(\cos\omega\phi_{\mathrm{a}} + \sin\omega\phi_{\mathrm{b}})(\cos\omega\bar{\phi}_{\mathrm{b}} + \sin\omega\bar{\phi}_{\mathrm{a}})| \\
&= \cos^2\omega|\phi_{\mathrm{a}}\bar{\phi}_{\mathrm{b}}| + \cos\omega\phi_{\mathrm{a}}\sin\omega\bar{\phi}_{\mathrm{a}} + \sin\omega\phi_{\mathrm{b}}\cos\omega\bar{\phi}_{\mathrm{b}} + \sin^2\omega|\phi_{\mathrm{b}}\bar{\phi}_{\mathrm{a}}| \\
&= \frac{1}{2}(1+\cos 2\omega)|\phi_{\mathrm{a}}\bar{\phi}_{\mathrm{b}}| + \frac{1}{2}\sin 2\omega|\phi_{\mathrm{a}}\bar{\phi}_{\mathrm{a}}| + \frac{1}{2}\sin 2\omega|\phi_{\mathrm{b}}\bar{\phi}_{\mathrm{b}}| + \frac{1}{2}(1-\cos 2\omega)|\phi_{\mathrm{b}}\bar{\phi}_{\mathrm{a}}| \\
&= \frac{1}{2}\sin 2\omega(|\phi_{\mathrm{a}}\bar{\phi}_{\mathrm{a}}| + |\phi_{\mathrm{b}}\bar{\phi}_{\mathrm{b}}|) + \frac{1}{\sqrt{2}}\left\{\frac{1}{\sqrt{2}}(|\phi_{\mathrm{a}}\bar{\phi}_{\mathrm{b}}| + |\phi_{\mathrm{b}}\bar{\phi}_{\mathrm{a}}|)\right\} + \frac{1}{\sqrt{2}}\cos 2\omega\left\{\frac{1}{\sqrt{2}}(|\phi_{\mathrm{a}}\bar{\phi}_{\mathrm{b}}| - |\phi_{\mathrm{b}}\bar{\phi}_{\mathrm{a}}|)\right\} \\
&= \frac{1}{2}\sin 2\omega({}^1\Phi_{\mathrm{ion\,a}} + {}^1\Phi_{\mathrm{ion\,b}}) + \frac{1}{\sqrt{2}}{}^1\Phi_{\mathrm{cov}} + \frac{1}{\sqrt{2}}\cos 2\omega{}^3\Phi_{\mathrm{cov}}
\end{aligned} \tag{6b}$$

$$|\mathrm{BSII}\rangle = |\psi^{-}_{\mathrm{HO}}\overline{\psi^{+}_{\mathrm{HO}}}| \tag{6c}$$

$$= \frac{1}{2}\sin 2\omega({}^1\Phi_{\mathrm{ion\,a}} + {}^1\Phi_{\mathrm{ion\,b}}) + \frac{1}{\sqrt{2}}{}^1\Phi_{\mathrm{cov}} - \frac{1}{\sqrt{2}}\cos 2\omega{}^3\Phi_{\mathrm{cov}} \tag{6d}$$

where other closed-shell MOs are neglected and ionic and covalent terms in the VB terminology are expressed by LMOs

$${}^1\Phi_{\mathrm{ion\,a}} = |\phi_{\mathrm{a}}\overline{\phi_{\mathrm{a}}}| \qquad {}^1\Phi_{\mathrm{ion\,b}} = |\phi_{\mathrm{b}}\overline{\phi_{\mathrm{b}}}| \tag{7a}$$

$${}^{1,3}\Phi_{\mathrm{cov}} = \frac{1}{\sqrt{2}}(|\phi_{\mathrm{a}}\overline{\phi_{\mathrm{b}}}| \pm |\phi_{\mathrm{b}}\overline{\phi_{\mathrm{a}}}|) \tag{7b}$$

The ion a(b) and cov configurations correspond, respectively, to an ionic pair and a covalent pair in the VB theory. The low-spin BS solutions are expressed with superposition of ionic and singlet covalent terms. Therefore, BS MO configurations BS I and BS II are different from the simple VB covalent term ${}^1\Phi_{\mathrm{cov}}$. In fact, BS MOs are regarded as a one-electron orbital description of the VB CI state, as shown in eq 6. This is the reason why we employ the universal MO (one-electron orbital)−VB (covalent electron pair) picture for explanation of electronic states of diradicals.[66] The BS MOs are indeed lucid and handy for construction of MO correlation diagrams for diradical reactions as in the case of the closed-shell MO description of nonradical reactions. However, the BS MO configurations involve a triplet covalent term ${}^3\Phi_{\mathrm{cov}}$ as an inevitable result of inclusion of a nondynamical electron correlation effect via the symmetry breaking. This broken symmetry term should be eliminated for recovery of spin symmetry in finite systems unless other factors such as spin−orbit interaction and external magnetic field play significant roles for real symmetry breaking.

The recovery of broken symmetry naturally resulted from the fact that BS I and BS II solutions are degenerate in energy and are not orthogonal, leading to the quantum mechanical resonance; note that the concept of resonance is one of the key concepts in the VB theory.[39] The in- and out-of-phase combinations of them indeed provide the pure singlet and triplet states, respectively.

$$\Phi_{\mathrm{SD}} = N(|\mathrm{BSI}\rangle + |\mathrm{BSII}\rangle) \tag{8a}$$

$$= \frac{1}{\sqrt{2(1+T^2_{\mathrm{HO}})}}\{\sqrt{2}\,{}^1\Phi_{\mathrm{cov}} + T_{\mathrm{HO}}({}^1\Phi_{\mathrm{ion\,a}} + {}^1\Phi_{\mathrm{ion\,b}})\} \tag{8b}$$

$$\Phi_{\mathrm{SD}} = N'(|\mathrm{BSI}\rangle - |\mathrm{BSII}\rangle) \tag{8c}$$

$$= {}^3\Phi_{\mathrm{cov}} \tag{8d}$$

where T_{HO} is the orbital overlap between BS MOs

$$T_{\mathrm{HO}} = \langle\psi^{+}_{\mathrm{HO}}|\psi^{-}_{\mathrm{HO}}\rangle = \sin 2\omega \tag{9}$$

The in-phase resonating BS MO state $|\mathrm{RBS}\,(+)\rangle$ in eq 8a is nothing but the approximate spin-projected (AP) BS solution after elimination of the ${}^3\Phi_{\mathrm{cov}}$ term. The AP energy correction is significant if the singlet and triplet energy gaps are large like those in the case of molecular oxygen (O_2) and isoelectronic Fe(IV)=O species.[40−42] The resonating BS state $|\mathrm{RBS}\,(+)\rangle$ reduces to the closed-shell solution $|\mathrm{RHF}\rangle$ (or RDFT) at the instability threshold of $\omega = \pi/4$.

$$|\mathrm{RHF}\rangle = \frac{1}{2}\{\sqrt{2}\,{}^1\Phi_{\mathrm{cov}} + ({}^1\Phi_{\mathrm{ion\,a}} + {}^1\Phi_{\mathrm{ion\,b}})\} \quad (10)$$

The RHF solution is responsible for the nonradical state in chemistry. Thus, a universal MO−VB description is the result when starting from BS MO calculations such as HF and KS DFT based on the independent particle model. On the other hand, the weight of the covalent term in eq 10 is always larger than that of the ionic term in the case of the VB CI and generalized VB (GVB) approaches even in the nonradical region because of inclusion of dynamical correlation

$$\Phi_{\mathrm{CI(2)}} = \cos\theta\,{}^1\Phi_{\mathrm{cov}} + \sin\theta({}^1\Phi_{\mathrm{ion\,a}} + {}^1\Phi_{\mathrm{ion\,b}}) \quad (\theta < \pi/4) \quad (11)$$

This VB CI expression is indeed nothing but a well-known Weinbaum formula[73] for the H_2 molecule, though a and b are AOs instead of LMOs.[71,72] MOs with RHF and RDFT are different from GVB orbitals in the nonradical region; note that GVB orbitals are indeed more or less diaradicaloid even for closed-shell bonds in the chemical sense.

The BS MO and BS MO CI results are often mapped into the Hubbard model,[74] where the transfer integral (t) and on-site Coulomb repulsion (U) have been employed as effective parameters to emphasize an important role of electron repulsion in extended systems. The Hubbard model is further reduced to the Heisenberg model,[75] where the effective exchange integral (J) is given with t and U parameters. The Hubbard model has been used to elucidate characteristics of potential curves of BS, RBS, and CI solutions.[66−72] In order to confirm the above Hubbard model, BS MO and resonating BS MO CI calculations of H_2 were performed using the ab initio UHF solution with the cc-pVTZ basis set. The potential curves obtained are shown in Figure 1. The computational results are wholly compatible with the above theoretical formulations and Hubbard model. The CI mixing of the RHF solution improves the cusp on the RBS(+) curve because of partial elimination of ionic terms (dynamical correlation). The BS MO and AP BS MO calculations of F_2 were also performed using ab initio UHF solution with the 6-31G basis set. It was found that the low-spin (LS) BS surface is repulsive in nature even in the short interatomic distance, but AP BS (UHF) improves the shape of the potential curve, providing the local minimum at $R = 1.6$ Å. The interatomic repulsion term between lone pairs should be added in the Hubbard model of fluorine. Thus, the RBS CI of diradicals indicated an important role of resonance between BSI and BSII configurations, leading to a universal MO−VB theory starting from the BS MO calculation;[66,76] note that AOs in the simple VB theory are replaced with BS MOs .

II.2. Quantum Resonance for Three-Spin Systems. Equilateral triangle systems have been regarded as typical spin frustrated systems, which are described by the so-called resonating VB (RVB) theory.[8,9] Therefore, it is interesting and important to extend a universal MO−VB theory to such systems. The symmery-adapted (SA) natural molecular orbitals for these systems are given by using site orbitals[66,77]

$$\phi_{\mathrm{S1(HONO)}} = \frac{1}{\sqrt{3}}(\phi_{\mathrm{a}} + \phi_{\mathrm{c}} + \phi_{\mathrm{b}}) \quad (12a)$$

$$\phi_{\mathrm{A(SONO)}} = \frac{1}{\sqrt{2}}(\phi_{\mathrm{a}} - \phi_{\mathrm{b}}) \quad (12b)$$

$$\phi_{\mathrm{S2(LUNO)}} = \frac{1}{\sqrt{6}}(\phi_{\mathrm{a}} - 2\phi_{\mathrm{c}} + \phi_{\mathrm{b}}) \quad (12c)$$

where singly occupied NO (SONO; SO) and LUNO (LU) are degenerate in energy. The BS MO solution responsible for spin structures **I** and **II** in eq 2 are given by the HONO−LUNO mixing as

$$\psi^{+}_{\mathrm{HO}} = \cos\theta\phi_{\mathrm{S1}} + \sin\theta\phi_{\mathrm{A}} \quad (13a)$$

$$\psi^{-}_{\mathrm{HO}} = \cos\theta\phi_{\mathrm{S1}} - \sin\theta\phi_{\mathrm{A}} \quad (13b)$$

$$\psi^{+}_{\mathrm{SO}} = \phi_{\mathrm{S2}} \quad (13c)$$

The BS axial spin density wave (ASDW) configurations (UHF in chemistry) with one-dimension (1D) spin structures **I** and **II** are expressed using these BS MOs

$$|\mathrm{BSI(ASDWI)}\rangle = |\psi^{+}_{\mathrm{HO}}\overline{\psi^{-}_{\mathrm{HO}}}\psi^{+}_{\mathrm{SO}}|$$
$$|\mathrm{BSII(ASDWII)}\rangle = |\psi^{-}_{\mathrm{HO}}\overline{\psi^{+}_{\mathrm{HO}}}\psi^{+}_{\mathrm{SO}}| \quad (14a)$$

$$|\mathrm{BSI(ASDWIII)}\rangle = |\psi^{+}_{\mathrm{HO}}(\mathrm{III})\overline{\psi^{-}_{\mathrm{HO}}}(\mathrm{III})\psi^{+}_{\mathrm{SO}}(\mathrm{III})| \quad (14b)$$

Therefore, spin densities at three sites are given with the orbital mixing parameter as

$$\rho_{\mathrm{a}}(\mathrm{SDWI}) = \frac{\sqrt{2}}{\sqrt{3}}\sin 2\theta + \frac{1}{6} = \rho_{\mathrm{b}}(\mathrm{SDWII}) \quad (15a)$$

$$\rho_{\mathrm{b}}(\mathrm{SDWI}) = -\frac{\sqrt{2}}{\sqrt{3}}\sin 2\theta + \frac{1}{6} = \rho_{\mathrm{a}}(\mathrm{SDWII}) \quad (15b)$$

$$\rho_{\mathrm{c}}(\mathrm{SDWI}) = \frac{4}{6} = \rho_{\mathrm{c}}(\mathrm{SDWII}) \quad (15c)$$

The spin densities obtained with BSI(ASDWI) and BSII(ASDWII) are consistent with classical structures **I** and **II**. On the other hand, the BS MO solution for BSIII(ASDWIII) is given by

$$\psi^{+}_{\mathrm{HO}}(\mathrm{III}) = \cos\theta\phi_{\mathrm{S1}} + \sin\theta\phi_{\mathrm{S2}} \quad (16a)$$

$$\psi^{-}_{\mathrm{HO}}(\mathrm{III}) = \cos\theta\phi_{\mathrm{S1}} - \sin\theta\phi_{\mathrm{S2}} \quad (16b)$$

$$\psi^{+}_{\mathrm{SO}}(\mathrm{III}) = \phi_{\mathrm{A}} \quad (16c)$$

The spin density that resulted from BSIII(ASDWIII) is given by

$$\rho_a(\mathrm{SDWIII}) = \frac{\sqrt{2}}{3}\sin 2\theta + \frac{1}{2} = \rho_b(\mathrm{SDWIII}) \tag{17a}$$

$$\rho_c(\mathrm{SDWIII}) = -\frac{2\sqrt{2}}{3}\sin 2\theta \tag{17b}$$

The spin densities with BSIII(ASDWIII) are also consistent with the spin structure **III**. The three BSX (X = I, II, and III) solutions are degenerate in energy at the triangle conformation corresponding to transition structures for exchange-forbidden radical insertion reactions.

On the other hand, the BS MO X (X = I−III) solutions with two-dimensional (2D) helical spin structure[4,5] are often constructed with complex molecular orbitals[66,77]

$$\phi_{HO} = \frac{1}{\sqrt{3}}(\phi_c + \phi_a + \phi_b) \tag{18a}$$

$$\phi_e = \frac{1}{\sqrt{3}}(\phi_c + \omega\phi_a + \omega^2\phi_b) = \frac{1}{\sqrt{2}}(\phi_{S2} - i\phi_A) \tag{18b}$$

$$\phi_{-e} = \frac{1}{\sqrt{3}}(\phi_c + \omega^2\phi_a + \omega\phi_b) = \frac{-1}{\sqrt{2}}(\phi_{S2} + i\phi_A) \tag{18c}$$

where $\omega = \exp(2/3\pi i)$. Three HSDW solutions are expressed with general spin orbitals (GSO) defined with complex MOs; for example, one of them is given by

$$\psi^{+}_{HO} = \cos\theta\phi_{HO}\alpha + \sin\theta\phi_e\beta \tag{19a}$$

$$\psi^{-}_{HO} = \cos\theta\phi_{HO}\beta + \sin\theta\phi_{-e}\alpha \tag{19b}$$

$$\psi_{SO} = \frac{1}{\sqrt{2}}(\phi_e\alpha + \phi_{-e}\beta) \tag{19c}$$

where α and β denote spin functions. The BS GSO solutions provide 2D (xy plane) spin density matrices, whose diagonal elements are given by

$$\rho_a(\mathrm{GSOI}) = \frac{-1}{6}(2\sin 2\theta + 1)(S_x - \sqrt{3}S_y) \tag{20a}$$

$$\rho_b(\mathrm{GSOI}) = \frac{-1}{6}(2\sin 2\theta + 1)(S_x + \sqrt{3}S_y) \tag{20b}$$

$$\rho_b(\mathrm{GSOI}) = \frac{1}{3}(2\sin 2\theta + 1)S_x \tag{20c}$$

The spin densities with eq 20 are consistent with GSOI structure, as illustrated in Scheme 5. Other GSOII and GSOIII solutions are also constructed with changing site orbitals in a cyclic manner. Then, each HSDW (BS GSO) solution exhibits the so-called triangular spin alignment (Néel state) in the field of solid state physics.[1−29]

SCHEME 5

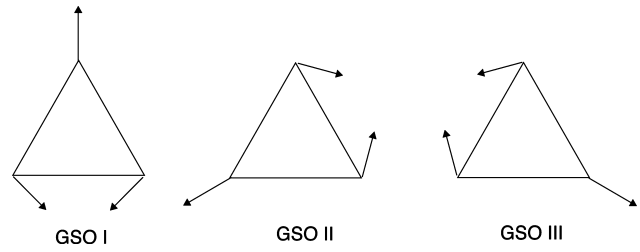

The resonating of three BS solutions is necessary for quantum spins with $S = 1/2$ because of strong spin frustration, in conformity with the resonating valence bond (RVB) concept by Anderson.[8,9] However, we here use the terminology resonating BS (RBS) CI since the basis configurations employed are BS MO and BS GSO solutions defined in eqs 13, 16, and 19. Since three BS MO solutions are degenerate in energy at the triangle conformation, the resonating BS MO CI wave function is expressed with the 3 × 3 CI form using three BS solutions as

$$\Phi_{CI(3)} = C_1|\mathrm{BSI}\rangle + C_2|\mathrm{BSII}\rangle + C_3|\mathrm{BSIII}\rangle \tag{21}$$

where C_i means the CI coefficient. RBS CI includes not only the covalent VB configurations in eq 1 and/or those in eq 2 constructed with LMOs (or AOs) but also several ionic VB terms as in the case of eqs 6 and 8 for two-spin systems. Then, BS MOs used in RBS CI are regarded as one-electron orbital expressions of the VB CI results for three-electron systems. In this sense, RBS CI includes three freedoms, spin, charge, and orbital, in the universal MO−VB description of strongly correlated electron systems, as illustrated in Figure 2. This means that RBS CI provides not only the nearest-neighbor effective exchange integrals (J) but also non-nearest-neighbor ones[78,79] in the spin Hamiltonian models, depending on the systems under consideration. The latter interactions often play important roles for determination of macroscopic properties, as shown below. For example, the cooperation of charge freedom in spin frustrated systems is now a current interest in relation to superconductivity.[23] RBS CI is thus applicable to derive reasonable model Hamiltonians for spin frustrated systems.[1−29]

II.3. Multiscale Multiphysics Simulation. The resonating GHF and HDFT (GSO) CI calculations for larger systems are impossible, leading to so-called multiscale multiphysics simula-

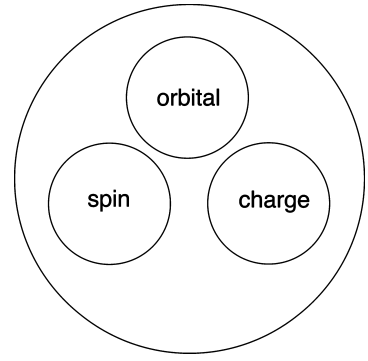

Figure 2. Orbital, spin, and charge freedom for strongly correlated systems. This means that RBS CI provides not only the nearest-neighbor effective exchange integrals (J) but also non-nearest-neighbor ones in the spin Hamiltonian models, depending on systems under consideration. The latter interactions often play important roles for determination of macroscopic properties.

tions in material science. In fact, phase transitions accompanied by long-range orders have been the main interest in infinite systems. However, suppression of such long-range order (symmetry breaking) is a current topic in frustrated systems.[27−29] In past decades, spin frustrated infinite systems such as triangular and kagome lattices have indeed been receiving continuous interest in the field of statistical physics. The magnetic properties of these systems have been investigated using the spin Hamiltonian

$$\hat{H}=-2\sum (J_{ij}^{x}S_i^{x}S_j^{x} + J_{ij}^{y}S_i^{y}S_j^{y} + J_{ij}^{z}S_i^{z}S_j^{z}) \qquad (22)$$

where it reduces to Ising (1D ($J_{ij}^{x} = J_{ij}^{y} = 0$ S_i^{z} − spin),[1−3] XY ($J_{ij}^{z} = 0$, 2D S_x and S_y spin),[7] or Heisenberg ($J_{ij}^{x} = J_{ij}^{y} = J_{ij}^{z}$, 3D spin) models.[12,13] No phase transition was concluded for the infinite Ising model of the triangular lattice because of the macroscopic degeneracy.[1−3] The long-range order of triangular spin alignment[4−6] in Scheme 5 was found for the XY model with a classical spin vector at zero temperature,[12] but the long-range order is destroyed at finite temperature. Monte Carlo (MC) simulations for the classical XY model indicated Korsterlitz and Thouless (KT)[7] and chirality[13] transition at finite temperature. The 120° spin rotation alignment in Scheme 5 was also the ground state for the triangular classical Heisenberg model at the zero temperature.[12] However, KT and chirality transitions were not predicted theoretically for the Heisenberg model at finite temperature. However, the classical MC simulation indicated a topological phase transition for the model.[12]

Spin wave (SW) theory and exact diagonalization calculations including quantum effects (fluctuation) indicated the stability of the 120° spin structure in the XY and Heisenberg models of the triangular spin lattice in the ground state.[15,18] However, exact diagonalization of the 36 spin system on the kagome lattice[17,27] indicated no energy spectra responsible for formation of magnetic order (for example, see Scheme 5) in the ground state, suggesting the nonmagnetic singlet (spin liquid) state.[20,28] Recently, spin liquid states were extensively examined in relation to the exotic superconductivity.[23−26,80] Thus, classical and quantum Heisenberg models play important roles for elucidation of magnetic properties of triangular and kagome lattices.

The above exact diagonalization calculations have been performed for finite quantum systems with the site spin number ($N \leq 36$) to elucidate spectral characteristics indicating long-range order in spin frustration systems. This indicates that both experimental and theoretical studies on mesoscopic systems with a triangular lattice are particularly interesting for elucidation of the nature of crossover and phase transition phenomena in spin frustrated systems. Synthesis of spin frustrated systems with mesoscopic size ($N < 100$) is indeed a challenge for chemists since such finite systems may become very interesting probes for physical characterizations. Several methods developed in the field of physical chemistry may be used for syntheses of these systems. On the other hand, two steps are necessary in multiscale multiphysics approaches to mesoscopic systems on theoretical grounds, (A) quantum chemical calculations of effective exchange parameters (J) and (B) exact diagonalization and/or quantum MC (QMC) simulation for searching exotic phases. First-principle calculation of J values is interesting and important for molecular design of mesoscopic spin frustrated systems.

The antiferromagnetic effective exchange interactions (J) in the Heisenberg models of spin frustration systems have been assumed as empirical parameters in the above statistical simulations. However, recent development of the hybrid Kohn−Sham density functional theory by the use of GSO enabled us to calculate J values even for spin frustration systems. The J value for the classical Heisenberg model is given by

$$J_{ab}^{C} = \frac{^{LS}E(\mathrm{GSO}) - {}^{HS}E(\mathrm{ASDW})}{3Ns^2} \qquad (23a)$$

where N and s mean the site number ($N = 3$) and size of local spin.[80−86] ^{LS}E(GSO) and ^{HS}E(ASDW) denote, respectively total energies of the low-spin (LS) GSO (triangular) HDFT and high-spin (HS) axial (1D spin) HDFT solutions. The GSO HDFT solution provides the spin density matrix which is characterized by 120° spin rotation, as shown in eq 20 and Scheme 5. On the other hand, the J value for the quantum Heisenberg model is given by eliminating the HS component from the LS GSO as

$$J_{ab}^{Q} = \frac{^{LS}E(\mathrm{GSO}) - {}^{HS}E(\mathrm{ASDW})}{^{HS}\langle S^2\rangle(\mathrm{ASDW}) - {}^{LS}\langle S^2\rangle(\mathrm{GSO})} \qquad (23b)$$

where $^{Y}\langle S^2\rangle$(X) denotes the total spin angular momentum of the spin state Y calculated with the method X. The total energy after this approximate spin projection (AP) is given by

$$^{LS}E(\mathrm{AP\ BSX}) = {}^{LS}E(\mathrm{BSX}) + J_{ab}^{Q}[{}^{LS}\langle S^2\rangle(\mathrm{BSX}) - 0.75] \quad (\mathrm{BSX} = \mathrm{ASDW, GSO}) \qquad (24)$$

where the second term is a quantum correction to the BSX (X = ASDW, GSO) solution. The magnetic properties of real systems are therefore investigated by using exact diagonalization of spin Hamiltonians constructed with effective exchange integrals determined with ab initio calculations and also with statistical simulation by the use of such ab initio spin Hamiltonians.

III. BS MO Calculations of Triangular Systems

III.1. Triangular Hydrogen Clusters. Hydrogen atom clusters are considered to be good theoretical models for spin frustration because the hydrogen atom has a quantum spin with $S = 1/2$. Previously,[80−86] we have examined several hydrogen clusters which are described with generalized Hartree−Fock (GHF) solutions by the use of general spin orbitals (GSO). For example, the odd-membered rings of hydrogen atoms H_n (n = 3, 5, 7, and 9) in A−D of Figure 3 were investigated with GHF (GSO) methods to elucidate possible helical spin structures.[4−6] The spin density vectors of these clusters were noncollinear, indicating the spin rotations with rotational angles of $\theta = 4\pi/n$. The spin structures were therefore consistent with those of the classical Heisenberg model with an equivalent intersite effective exchange integral with negative sign ($J < 0$; antiferromagnetic). The triangular ladder systems constructed with hydrogen atoms H_n (n = 3, 5, 7, and 9) were also investigated with GHF (GSO) to evaluate effective exchange interactions (J) as illustrated in E−G of Figure 3. Recently, triangular tubes in H and I have also accepted great interest. The numbers of configuration state functions (CSF) with the smallest S_z number[31,86] are, respectively, 3, 10, 35, and 125 for 3, 5, 7, and 9 spin clusters. Each BS MO solution for RBS CI can be constructed for three-spin systems. However, the construction of BS MO solutions is almost impossible for larger spin clusters ($N > 3$).

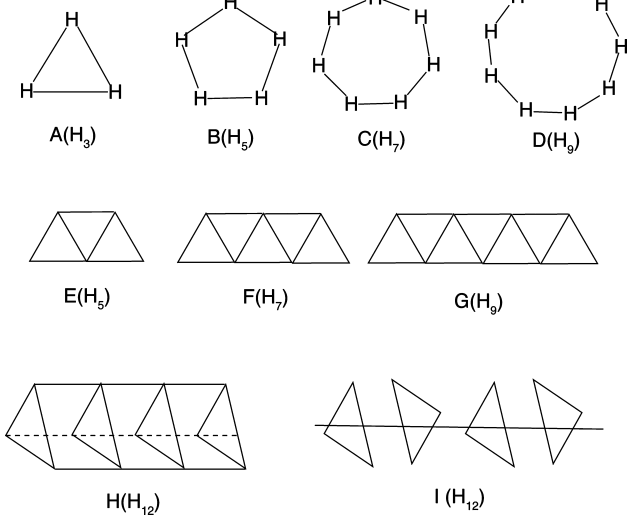

Figure 3. Spin frustrated systems: odd-membered cyclic hydrogen clusters (A−D), triangular ladders (E−G), and triangular tubes (H, I). Hydrogen atom clusters are considered to be good theoretical models with spin frustration because the hydrogen atom has a quantum spin with $S = 1/2$.

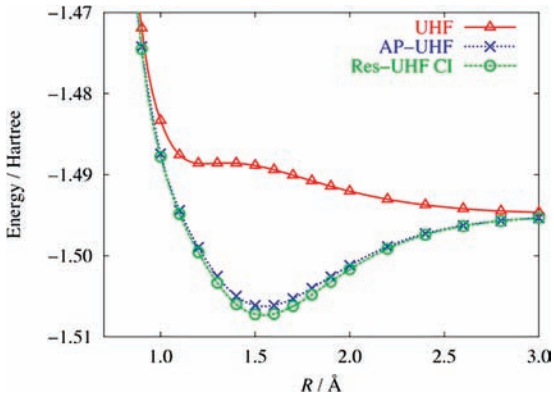

Figure 4. Potential curves of three hydrogen clusters with the triangle conformation calculated with UHF (ASDW), AP UHF, and resonating UHF CI methods. The potential curve for the doublet UHF solution is repulsive in nature because of the inclusion of the quartet component as a broken symmetry configuration. On the other hand, the resonating UHF CI surface indicates the bound state near $R \approx 1.5$ Å, showing remarkable improvement. The spin-projected UHF obtained with elimination of the quartet component via the AP procedure also provides a bound surface which is close to the resonating UHF CI surface.

The spin-optimized (SO) resonating BS (RBS) CI procedures have been proposed for such systems on the basis of the Löwdin spin projection scheme for generation of CSFs from the most stable BS MO solution.[84−86] The SO RBS CI is applicable even for large systems taking into account only lower excited configurations.

Here, the 3 × 3 RBS CI in eq 21 was carried out for the triangle H_3 radical, changing the interatomic distance R(Å) in order to employ the universal MO−VB approach for spin frustrated systems. Figure 4 illustrates the calculated potential curves using the axial SDW (namely, conventional UHF) solutions by use of the cc-pVTZ basis set. The potential curve for the doublet UHF solution is repulsive in nature because of the inclusion of the quartet component as a broken symmetry configuration. On the other hand, the 3 × 3 resonating UHF CI surface indicates the bound state near $R \approx 1.5$ Å, showing remarkable improvement because of exact elimination of the quartet component. The spin-projected UHF obtained with

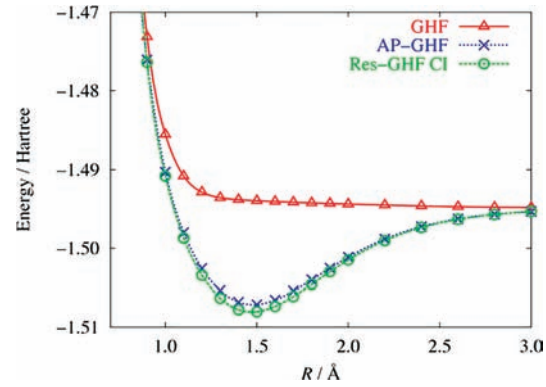

Figure 5. Potential curves of three hydrogen clusters with the triangle conformation calculated with GHF(GSO), AP GHF, and resonating GHF CI methods. The GHF potential curve is almost flat, indicating no minima like in the case of the UHF surface. On the other hand, resonating GHF CI provides a minima on the potential curve near $R \approx 1.5$ Å. The AP GHF surface is also close to that of the resonating GHF CI, indicating the utility of the AP procedure for practical purpose. The resonating GHF CI surface is more stable than the resonating UHF CI one in the region of local minima.

elimination of the quartet component via the AP procedure in eq 24 also provides a bound surface which is close to the resonating UHF CI surface. The AP procedure is necessary even for qualitative purpose in this system. Thus, quantum resonance of three BS (UHF) solutions is essential for theoretical description of the triangle H_3 radical, compatible with the RVB theory of the spin frustration system.[8,9]

The general Hartree−Fock (GHF) with general spin orbitals (GSO) responsible for helical spin structure in Scheme 5 is always more stable than UHF with axial spin structure (Scheme 2) because of spin frustration, as shown in Figure 5. However, the GHF (GSO) potential curve is almost flat, indicating no minima like those in the case of the UHF surface. On the other hand, 3 × 3 resonating GHF (GSO) CI provides a minima on the potential curve near $R \approx 1.5$ Å. The AP GHF (GSO) surface is also close to that of the resonating GHF (GSO) CI, indicating the utility of the AP procedure for practical purpose. The resonating GHF CI surface is more stable than the resonating UHF CI one in the region of local minima. This means that the spin correlation expressed with triangular spin structure is retained even in dynamical rotations of spins via quantum fluctuation in the case of geometrically frustrated systems. Such spin correlation is indeed realized as triangular spin alignment in triangular lattice.

The computational results in Figures 4 and 5 clearly indicate the necessity of elimination of the quartet component via the resonating CI and/or AP procedure. The weight of the quartet (high-spin) component can be estimated with the total spin quantum number $\langle \hat{S}^2 \rangle$ obtained with the BS MO calculations. Figure 6 illustrates variation of $\langle \hat{S}^2 \rangle$ values with UHF (ASDW) and GHF (GSO) solutions before and after 3 × 3 resonating CI in the course of the dissociation reaction. The $\langle \hat{S}^2 \rangle$ values with the BS MO are larger than the exact doublet value (0.75), indicating significant contribution of spin contamination ($\langle \hat{S}^2 \rangle = 3.75$ for the quartet state), particularly in the dissociation region ($R > 2.0$ Å). The magnitude of the spin density in eq 20 becomes 1.0 at the dissociation limit, indicating the formation of three atomic hydrogens. The $\langle \hat{S}^2 \rangle$ values at the local minima ($R \approx 1.5$ Å) remain to be 1.20−1.25, showing the non-negligible contribution of the contamination error. The resonating BS MO CI removes such an error exactly as shown in Figure 6. This is consistent with remarkable improvement of the potential curves in Figures 4 and 5.

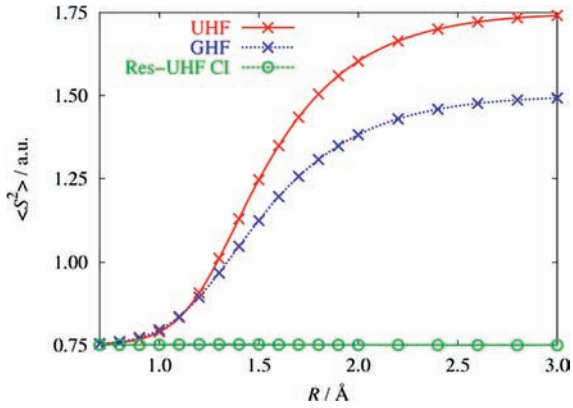

Figure 6. Variations of the total spin angular momentum with the increase of the interatomic distance calculated with UHF, GHF, and resonating UHF (GHF) CI methods. The $\langle \hat{S}^2 \rangle$ values with BS MO are larger than the exact doublet value (0.75), indicating significant contribution of spin contamination, particularly in the dissociation region ($R > 2.0$ Å). The $\langle \hat{S}^2 \rangle$ values at the local minima ($R \approx 1.5$ Å) remain to be 1.20−1.25, showing the non-negligible contribution of the contamination error. The resonating BS MO CI removes such an error exactly.

III.2. Tris(methylene) Amine. The resonating VB (RVB) state received renewed interest after the discovery of high-T_c superconductivity of cuprates. Such discovery indeed enabled us to consider a spin-mediated mechanism of superconductivity instead of the charge-mediated mechanism proposed by Little.[87] For example, the molecular structures of bis(methylene) and tris(methylene) amines were considered as organic isoelectronic analogues of the copper oxygen bond in cupurates just after the discovery of the high-T_c superconductivity[88,89] on the basis of strong superexchange interaction ($|J| \gg 0$) between localized spins.

$$\mathrm{Cu(II)-O^{2-}-Cu(II)} \leftrightarrow \mathrm{R_2C^{\cdot}-X-C^{\cdot}R_2} \quad (\mathrm{X = NR', N-C^{\cdot}R_2}) \qquad (25)$$

The tris(methylene) boron skeletons (X = BR′) were also proposed as another isoelectronic bond to the copper oxygen bond. The triangular structure can be constructed in the case of boron-doped diamond superconductors. These skeletons have been regarded as organic component units of molecules (A), polymers (B), sheets (C), and tubes (D) with triangular spin structures as shown in Figure 7. These species would be possible candidates for exotic materials with an antiferromagnetic (Neel order, one of broken symmetry state)) state, a spin liquid state with no symmetry breaking, and a superconductivity state via the so-called RVB theory.[26] The superexchange integral (J) was utilized to estimate the transition temperature for the antiferromagnetic order, spin gap, and superconductivity in our J model.

We here investigated the smallest unit, tris(metylene)amine, as an example of organic spin frustrated systems as shown in Figure 7A. Figure 8 illustrates the potential curves with low-spin (LS) GHF (GSO) and quartet (high-spin (HS)) UHF (ASDW) solutions with the 4-31G basis set along the elongation path of the nitrogen (N) and carbon (C) distance (R). The LS GHF (GSO) was more stable than the HS UHF (ASDW) in the whole region ($1.0 \le R \le 1.9$ Å). The local minima on the surface were also found at $R \approx 1.37$ Å for LS GHF and $R \approx 1.40$ Å for HS UHF (ASDW).

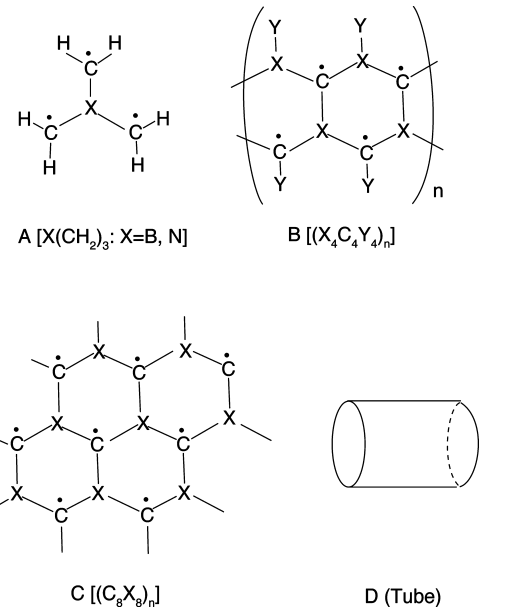

Figure 7. Spin frustrated systems consisting of $X(CH_2)_3$ (X = N, B, ...) systems (A), a one-dimensional (1D) polymer; (B) a two-dimensional (2D) sheet (C), and a three-dimensional (3D) tube (D).

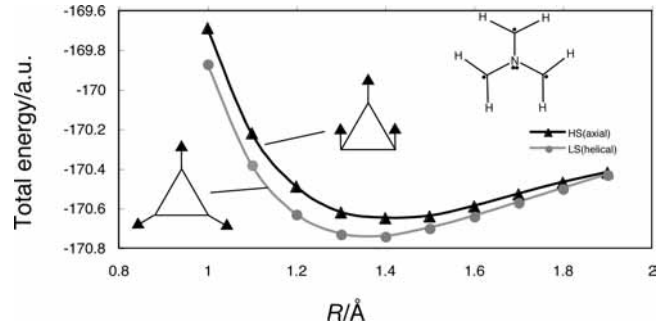

Figure 8. Potential curves of the low-spin (LS) GHF(GSO) and high-spin (HS) UHF (ASDW) states of $N(CH_2)_3$ with a change of the C−N distance (R). The LS GHF (GSO) was more stable than the HS UHF (ASDW) in the whole region ($1.0 \le R \le 1.9$ Å). The local minima on the surface were also found at $R \approx 1.37$ Å for LS GHF and $R \approx 1.40$ Å for HS UHF (ASDW).

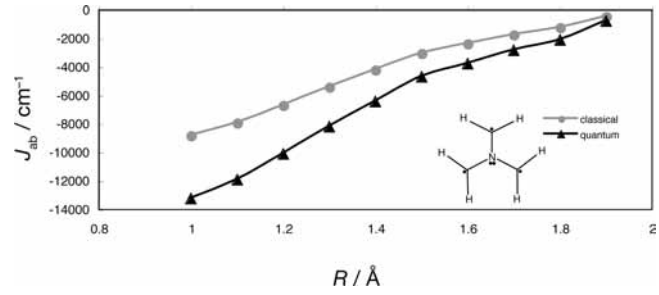

Figure 9. Variations of effective exchange integrals of $N(CH_2)_3$ calculated with LS GHF and HS UHF energies under classical and quantum approximations (see eq 23a) with the change of the C−N distance. The ${}^{C}J_{ab}$ and ${}^{Q}J_{ab}$values are negative in sign, indicating the predominant role of the superexchange interaction. The magniude of $|{}^{Q}J_{ab}|$ was larger than that of $|{}^{C}J_{ab}|$ in the whole region.

The effective exchange integrals (J) between methylene radical sites via the nitrogen lone pair were calculated using classical and quantum Heisenberg models as shown in eqs 23a and 23b. Figure 9 shows variations of classical (${}^{C}J_{ab}$) and quatum (${}^{Q}J_{ab}$) effective exchange integrals with changing R. The ${}^{C}J_{ab}$ and ${}^{Q}J_{ab}$values are negative in sign, indicating the predominant role of the superexchange interaction. The magniude of $|{}^{Q}J_{ab}|$

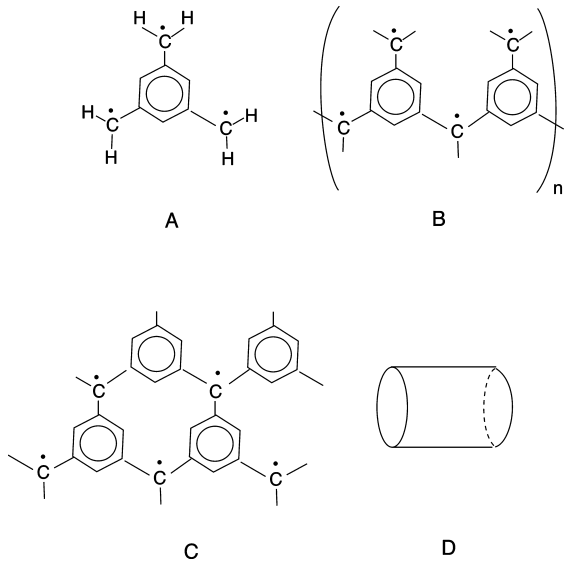

Figure 10. Spin frustrated systems consisting of 1,3,5-trimethylbenzene (A), a one-dimensional (1D) polymer (B), a two-dimensional (2D) sheet (C), and a three-dimensional (3D) tube (D).

was larger than that of $|^{C}J_{ab}|$ in the whole region. This is a reverse tendency that $|^{Q}J_{ab}|$ becomes smaller than $|^{C}J_{ab}|$ in the case of the pure covalent VB configuration. The mixing of the ionic terms responsible for superexchange interaction plays an important role in this system, leading to large $|J|$ values. Since these J values are indeed 4000−6000 cm^{-1} even at the equilibrium distance, the superexchange integral for the tris(methylene) unit is larger than twice the $|J|$ value for the copper oxygen bond. This may imply that several transition temperatures estimated with J are quite high in the organic materials with doped holes (X = N) and electrons (X = B) in Figure 7. Chemical synthesis of the triangular network consisting of the C−N unit is desirable using physical methods. The situations are the same for the carbon−boron systems, which are partly realized in the boron-doped diamonds, a possible candidate for high-T_c superconductor.

III.3. 1,3,5-Tris(methylene)benzene. Doping of holes or electrons into molecule-based materials with ferromagnetic interaction is one of the interesting problems in molecular magnetism and spin-mediated superconductivity.[88−91] In fact, 1,3,5-tris(methylene)benzene has been considered as a component unit for molecules (A), oligomers and polymers (B), sheets (C), and tubes (D) with high-spin (ferromagnetic) ground states, as shown in Figure 10. The ferromagnetic exchange interactions ($J \gg 0$) between methylene groups via a *meta*-phenylene bridge have been thoroughly investigated using symmetry-adapted (SA) CAS and BS hybrid DFT (HDFT) methods.[92,93] Both SA CAS and BS HDFT calculations concluded that the spin polarization (SP) effect instead of the superexchange interaction plays a predominant role in the stabilization of the high-spin states in exotic materials in Figure 10. This implies that the low-spin states with spin frustration become excited states in these systems.

We performed the BS MO calculations of 1,3,5-tris(methylene)benzene using the 4-31G basis set as a unit of molecular materials in Figure 10. The UHF(ASDW) solution with quartet configuration (high-spin (HS)) was far more stable than the GHF(GSO) solution with doublet (low-spin (LS)) configuration. The spin densities calculated with these BS MO solutions indicated the spin polarization effects as illustrated in Scheme 6. The effective exchange (J) integrals were calculated with total

SCHEME 6

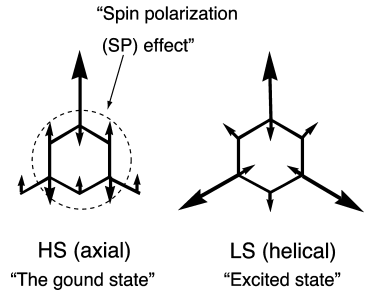

energies and total spin angular momentums of the HS and LS BS solutions (see eq 23). The classical and quantum J values were 1446 and 1452 (cm^{-1}), showing the ferromagnetic interaction. These calculated results are compatible with previous computational results for related materials such as 1D ferromagnetic polymers, 2D ferromagnetic sheets, and ferromagnetic tubes in B, C, and D of Figure 10. The very large $|J|$ value is promising for construction of the high-T_c organic ferromagnets, though their chemical syntheses by the use of photochemical methods are still difficult. Suppression of the high reactivity of triplet carbene sites is important for the purpose.

III.4. Tris(methylene) Cluster. Spin frustration via quantum effects is known to be dependent on the size of component spins; note that systems with the 1/2 spin at each site are best candidates for the spin liquid state because of strong spin frustration, as illustrated in Figures 3 and 7. On the other hand, triangular spin structures may be realized in the case of molecular materials with much larger spins ($S > 1/2$) at each site, as shown in Figure 11. The number of spin states for N-site clusters with spin size is given by $(2S + 1)^N$, and then, it becomes close to the thermodynamic limit if S is large. The triplet methylene group is considered a magnetic site with triplet

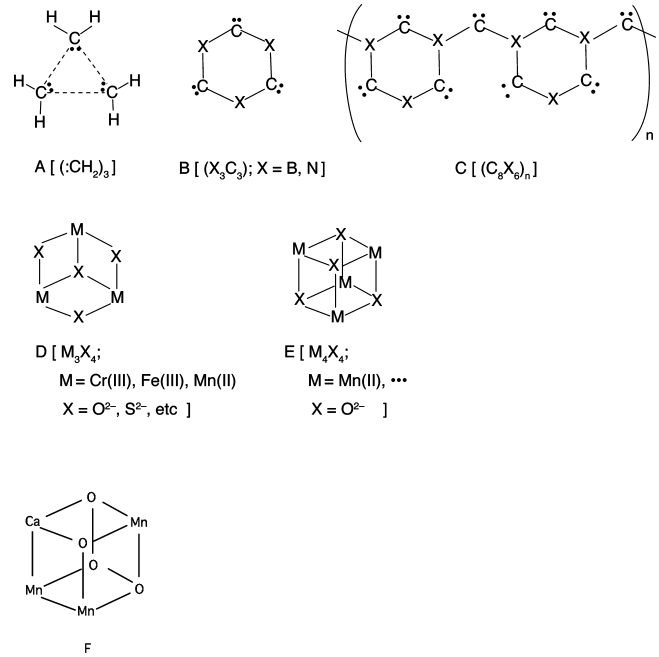

Figure 11. Spin frustrated systems constructed of a triplet carbene group; (A) triangle system with through-space interaction, (B, C) triangle system with through-bond interaction and 1D polymer and spin frustrated systems constructed of transition-metal complexes, (D) triangles with superexchange interaction, and (E) cubanes with antiferromagnetic interaction. (F) Triangular $Mn(II)_3CaO_4$, where Mn(II) ion was replaced with a divalent Ca ion in (E).

($S = 1$) spin. Here, an equilateral triangle consisting of triplet methylene was examined by changing the intermolecular distance as an example of a spin frustrated system in Figure 11. Potential curves obtained with low-spin (LS) GHF (GSO) and high-spin (HS) ($S = 3$) UHF (ASDW) solutions are given in the Supporting Information, Figure S3. The LS GHF surface was more stable than that of HS UHF surface in the whole region examined. The HS surface was repulsive, but the LS surface exhibited a local minimum at $R = 1.1$ A. The ${}^{C}J_{ab}$ and ${}^{Q}J_{ab}$values were also calculated using total energies and total angular momentums as shown in eq 23. Both J values were negative (antiferromagnetic) in nature. The magnitude of the ${}^{Q}J_{ab}$ value was smaller than that of ${}^{C}J_{ab}$ value, as expected from the direct exchange interaction between local spins.

The computational results for the tris(methylene) cluster suggest that a triangular ladder may be constructed with a triplet carbene unit, as shown in Figure 11C. However, a triplet carbene site is usually highly reactive to undergo radical coupling reactions. Therefore, many efforts have been performed to stabilize triplet carbene units in this field, as discussed previously.[92,93] On the other hand, nitroxide and nitronyl nitroxide have been employed as stable $S = 1/2$ radical units. Their high-spin dimer with $S = 1$ can be used as a component for construction of spin frustrated systems. Awaga et al. have reported that the *m*-MPYNN^{+} dimer has triplet ground state, forming a kagome lattice constructed of corner-shared triangles.[17] The observed intra- and interdimer effective exchange integrals were 11.3 and -1.2 K, respectively, for this kagome lattice. The spin frustration character was found even for the $S = 1$ pure organic kagome lattice.[17] This may imply that organic diradicals with triplet ground state are good components for construction of organic spin frustration systems since spin−orbit interactions are relatively weak for the species.

III.5. Trinuclear Transition-Metal Complexes. The transition-metal ions (M) with local spin have been used to construct triangular complex, for example, M = Cr(III) with $S = 3/2$, Fe(III) with $S = 5/2$, and Mn(II) with $S = 5/2$, as shown in Figure 11D. The cubane-type cluster in Figure 11E and the triangular tube in Figure 3 are also interesting transition-metal complexes with spin frustration. Recently, several triangular and kagome lattices consisting of transition-metal complexes have indeed been realized and characterized with physical observations as described below.[94−106] We have already examined several spin frustrated systems consisting of several transition-metal ions. The classical Heisenberg (spin vector) model was used to elucidate possible spin structures in part II of this series, assuming negative (antiferromagnetic) effective exchange interactions. The magnetic group-theoretical considerations of cubane-type 4Fe-4S clusters have been performed to elucidate possible electronic structures with collinear and noncollinear spin densties.[107] The J values were also calculated for triangle and hexagon clusters of Co(IV) ions in the CoO_2 superconductors,[80,81] triangle, tetrahedron, and trigonal-bipyramid clusters of Cr atoms,[108] and the cubane-type Mn(II) cluster, $Mn(II)_4O_4$ in E of Figure 11, using the GHF and GDFT GSO methods.[109]

Here, the triangular $Mn(II)_3CaO_4$ cluster in Figure 11F, where the Mn(II) ion was replaced with the divalent Ca ion in the cubane cluster (E of Figure 11) in the oxygen evolution center (OEC), was examined as an example. Used basis sets are all electron basis sets of valence double-ζ (DZ) quality (Huzinaga's MIDI for iron atoms and Pople's 6-31G for hydrogen and sulfur atoms). The employed XC functional was a hybrid one (B3LYP) using the HFS and VWN5 correlation functionals and the Becke88 and LYP correlation functionals. The XC functional was numerically integrated utilizing a pruned integral grid of 75 radial shells and 305 angular points per shell. All SCF energies were converged within 10^{-7} au. Magnetic interactions of the $Mn(II)_3CaO_4$ cluster can be described by the Heisenberg spin Hamiltonian, assuming that Mn(II) spin orbitals are localized on each Mn(II) centers. Three spin states were considered, ferromagnetic (F), antiferromagnetic (AF), and noncollinear (NC) states. The F state is a highest spin state of $S = 15/2$, the AF state is a broken symmetry state of $S_z = 5/2$, and the NC state has $S_z = 1/2$, where the local spins are aligned at 120° with each other in one plane. Neglecting orbital overlaps between localized spin orbitals, $\langle S^2 \rangle$ values are ${S^2}_{F} = 63.75$, ${S^2}_{AF} = 13.75$, and ${S^2}_{NC} = 7.5$ for F, AF, and NC states, respectively.

Approximate spin correlation functions between spin centers can be evaluated from the following equations under the generalized spin projection approach.

$$\begin{aligned} \langle S^2 \rangle_{\text{Spin State}} &= \sum_{i}^{i=1,2,3} \langle S_i^2 \rangle + \sum_{i,j\neq i}^{i=1,2,3} \langle S_i \cdot S_j \rangle_{\text{Spin State}} + \delta \langle S^2 \rangle^{\text{sp}} \\ &= 3\left(\frac{5}{2}\cdot\frac{7}{2}\right) + 3\langle S_i \cdot S_j \rangle_{\text{Spin State}} + \delta \langle S^2 \rangle^{\text{sp}} \end{aligned} \tag{26}$$

where $\delta\langle S^2 \rangle^{\text{sp}}$ is a small positive value arising from a spin polarization effect in unrestricted calculations. Using eq 26, spin correlation functions between neighboring spin centers are estimated from calculated $\langle S^2 \rangle$ values such as ${}^{F}\langle S \cdot S \rangle_{\text{ForAF}} = 6.25$ (for ferromagnetically coupled pair in F and AF state), ${}^{AF}\langle S \cdot S \rangle_{AF} = -6.456$ (for the antiferromagnetically coupled pair in AF state), and $\langle S \cdot S \rangle_{NC} = -3.286$ (in the NC state). Compared to the spin correlation function of $\langle S \cdot S \rangle_{S=1/2} = -4.25$ in the ground $S = 1/2$ spin state, the spin correlation function in the NC state is much closer than that in the AF state. The NC state becomes the ground state.

The J values can be calculated using eq 23. It was confirmed that the most stable state is NC, which is slightly lower than AF. Thus, the $Mn(II)_3CaO_4$ cluster is concluded to be a typical frustrated antiferromagnetic system, as expected by the spin Hamiltonians. For the small energy gap between AF and NC states, calculated J values from F−AF and F−NC are similar, $J_{F-AF} = -50.8$ cm^{-1} and $J_{F-NC} = -61.0$ cm^{-1}; note that the average is $J_{AVE} = -55.9$ cm^{-1}. The AF solution corresponds to the $S_z = 5/2$ state of the $Mn(II)_3CaO_4$ cluster, whereas the NC solution is an approximation of the lowest spin state ($S_z = 1/2$). Therefore, the NC state becomes more stable than the AF state. The noncollinear spin structure in the NC state is in a 2D ($S_y = 0$) supported approximate triangle structure with classical spin−spin angles of $\theta_{12} = \theta_{23} = \theta_{31} = 120.0°$; note that the S_y component becomes zero for real GSO, in contrast to eq 20.[63] Spin polarizations on the ligands take noncollinear spin density, reflecting the terminating Mn(II) ion. The natural orbital analysis of the GSO B3LYP solution was also performed to elucidate the nature of molecular orbitals and their occupation numbers.

Natural orbitals (NOs) in the NC state are delocalized over the whole molecule, mainly concentrated on Mn(II) centers, as shown in Figure 12. The occupation numbers of natural orbitals are also shown in the Figure 12. The occupation numbers of five singly occupied orbitals in the AF (collinear) solution are not 1.0 in the case of NC state, where the HONO and LUNO are a higher occupied natural orbital with $n_i > 1$ and a lower occupied natural orbital with $n_i < 1$, respectively; note that orbital symmetry pairings in the AF state for HONO−LUNOs are not

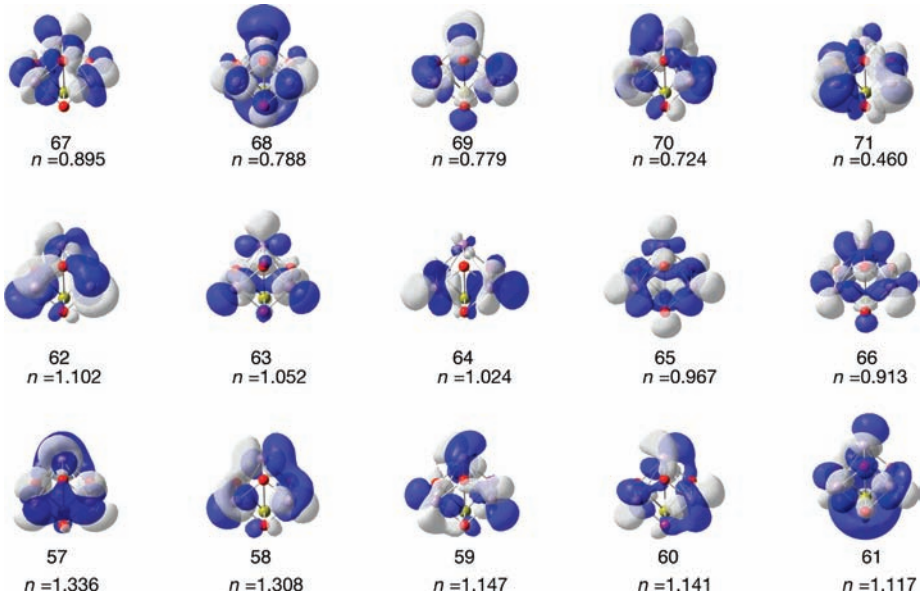

Figure 12. Natural orbitals and occupation numbers of the $Mn(II)_3CaO_4$ systems with spin frustration obtained with GSO DFT calculations. The occupation numbers of five singly occupied orbitals in the AF (collinear) solution are not 1.0 in the case of the NC state, where HONO and LUNO are a higher occupied natural orbital with $n_i > 1$ and a lower occupied natural orbital with $n_i < 1$, respectively.

seen in the NC state because of the orbital−spin mixing, as shown in eq 19. A slower decrease of the NC occupation numbers clearly shows the difference of electron correlations for these natural orbitals. Chemical indices such as the information entropy are also calculated with the occupation numbers (Supporting Information, Table S3).

IV. Results and Discussions

IV.1. Exact Diagonalization of Heisenberg Hamiltonians. The GHF and GDFT GSO computations of large clusters are not so easy even now. Moreover, computations of the spin excited states with intermediate total spin numbers are impossible within the single determinant theory. Then, as shown in section III, the GHF and GDFT GSO computational results were mapped on the effective spin Hamiltonians to elucidate the spin liquid state of spin frustrated systems. Here, exact diagonalization of the Heisenberg spin Hamiltonians was performed for spin clusters illustrated in A−D of Figure 13. These models, for example, correspond to typical spin frustrated systems, (A) a hexagon cluster for the CoO_2 superconductor, (B) a triangular cluster for the κ-$(KEDT-TTF)_2Cu_2(CN)_3$[23] and β'-$Me_4P[Pd(dmit)_2]_2$[22] superconductors, (C) a triangle−pentagon cluster for a spin polyhedron $Mo_{72}V(IV)_{30}$ with coners sharing triangle network,[110−120] and (D) a kagome lattice cluster for the Cu(II) compounds with a kagome lattice. Figure 14 shows the calculated energy diagrams for A−D clusters with antiferromagnetic interaction (J) between the $S = 1/2$ spin components; note that the energy levels are normalized with J.

The ground states of these clusters were the lowest spin states with singlet pairing, $S_{total} = 1/2$ for A and B and $S_{total} = 0$ for C and D in Figure 13, in accord with the experimental results (see below). The ground singlet states of C or D are degenerate in energy because of strong spin frustration. A lot of degeneracy is also observed in the excited states of the total lowest and next lowest spin states of B, C, and D. The lowest excited state of A and B clusters was a spin−unflip doublet ($S_{total} = 1/2$), while that for C and D clusters was a spin−flip triplet with $S_{total} = 1$, as shown in Figure 14. The energy gap was not zero for any of the clusters examined. This indicates that the excitation energy is necessary for breaking the singlet pairing

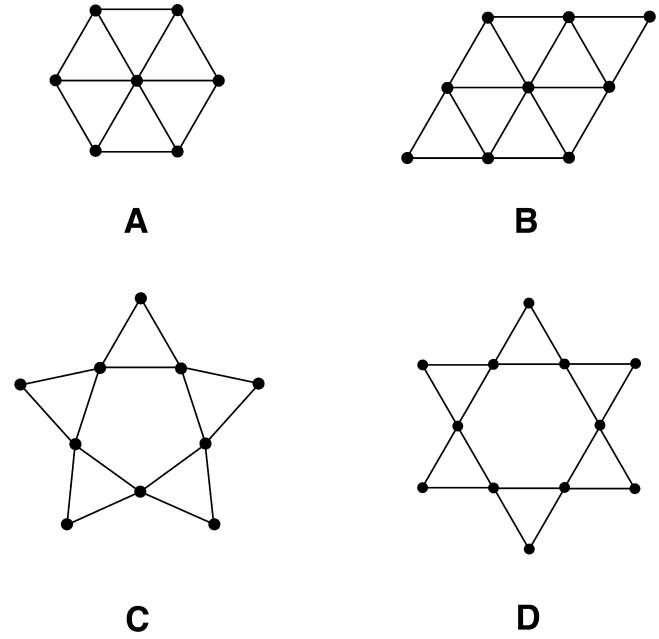

Figure 13. Spin frustration systems for quantum Heisenberg models: (A) hexagone, (B) triangular lattice, (C) triangle-pentagon cluster, and (D) kagome lattice cluster.

of the spin ball $Mo_{72}V(IV)_{30}$ (C) and the kagome lattice $ZnCu_3(OH)_6Cl_2$ (D) if the idealized geometrical frustrations are realized without lattice deformations, though the experimental results indicated some deviations.

The magnetic susceptibility curves were calculated changing the magnitude of the antiferromagnetic effective exchange interactions, $J = -40$, -400, and -4000 cm^{-1} for the clusters A−D in Figure 13. The calculated results are shown in Figure 15. The magnetic susceptibility in the range of $T < 300$ K was constant for A and B and zero for C and D for the very strong antiferromagnetic case with $J = -4000$ cm^{-1}, which corresponds to the magnetic materials constructed with $N(CH_2)_3$, as shown in Figure 7. The magnetic susceptibility for C and D was developed in the higher temperature region ($T > 100$ K) for the case with $J = -400$ cm^{-1}, showing similar behavior to

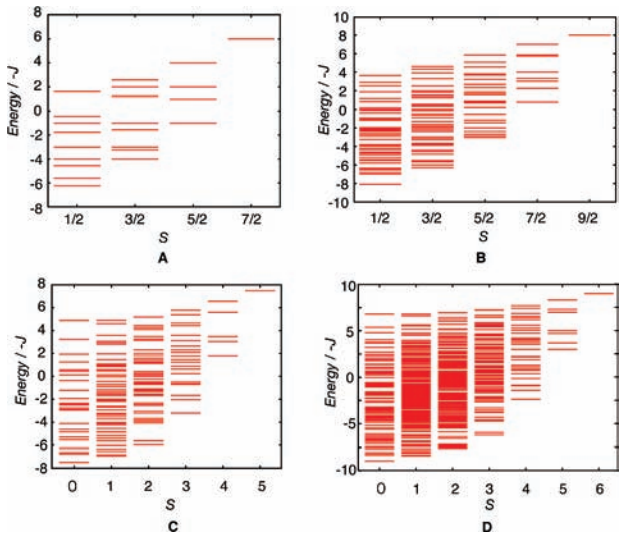

Figure 14. Energy levels obtained with exact diagonalization of the Heisenberg model for model clusters (A−D) in Figure 13 with spin frustration. The ground states of these clusters were the lowest spin states with singlet pairing; $S_{total} = 1/2$ for (A) and (B), and $S_{total} = 0$ for (C) and (D). The ground singlet states of (C) or (D) are degenerate in energy because of strong spin frustration.

that of iron sulfide clusters in ferrodoxins.[107] On the other hand, the magnetic susceptibility exhibited typical antiferromagnetic behavior for the weak antiferromagnetic case $J = -40$ cm^{-1}, which, for example, corresponds to the manganese cluster $CaMn_3O_4$ examined here. The magnetic susceptibility for C and D clusters reduced to zero at low temperature, in agreement with the spin gap in the spin liquid state. However, the magnetic susceptibility curve did not show the so-called 1/3 plateau within the uniform Heisenberg model, indicating the necessity of the anisotropic term such as the Dzyaloshinski−Moriya term for anomaly (see below).

IV.2. Spin Frustration Systems. As shown in Schemes 1−5, the triangle system has the degenerate total doublet and excited quartet state. The spin transition between the doublet and quartet states occurs under the external magnetic field. Recently, chemical synthesis of odd-membered rings has received great interest. Triangle systems have indeed been realized for characterization of magnetic properties with high-field electron paramagnetic resonance (ESR), magnetic susceptibility measurements, and neutron diffraction methods. Choi et al. have performed the high-field pulsed ESR experiments on $Na_9[Cu_3Na_3(H_2O)_9(\alpha\text{-}AsW_9O_{33})_2]\cdot 26H_2O$,[94,95] namely, the triangular {Cu(II)$_3$} system, where Cu(II) ($S = 1/2$) ions are antiferromagnetically coupled, a typical triangle nanomagnet. Their ESR experiments showed that the magnetization first exhibits a plateau at around 1.15 μ_B, then jumps to 2.6 μ_B, and finally approaches gradually to the saturation value of 3.4 μ_B in the high field of 13 T. The first step corresponds to the saturation of $S_{total} = 1/2$, and the second step comes from the level crossing between total 1/2 and 3/2 states. Thus, the energy levels determined by ESR also unveiled that the different mixing nature of the spin chirality of a total $S = 1/2$ Kramers doublet by virture of a Dzyaloshinski−Moriya (DM) interaction is decisive for inducing half-step magnetization. Yoneda et al. synthesized an iron−oxygen compound $[Fe(II)(\mu\text{-bpypz}_3)_2Fe(II)(\mu_3\text{-}O)]^{2+}$,[96] which involves the triangle ring $[Fe(II)_3O]^{4+}$ core. The Mössbauer experiments demonstrated the high-spin (HS) ground state of Fe(II) ($S = 2$). The temperature dependence of the magnetic susceptibility indicated that the J value between Fe(II) ions is -29.0 cm^{-1}, compatible with the simple triangle model.

In past decades, odd-membered rings have been considered as spin frustration systems.[33−35] However, chemical synthesis of such systems has been difficult. Cador et al.[97] synthesized an odd-membered (total nine) ring $[(C_6OH_{11})_2NH_2][(Cr_8NiF_9)_{18}]]$ consisting of eight Cr(III) ($S = 3/2$) ions and one Ni(II) ($S = 1$) ion, Cr_8Ni. The ESR experiment by them demonstrated that the frustration is delocalized on the Cr(III) chain while the antiparallel alignment is more rigid at the nickel site. Probably, several examples of odd-membered spin frustration systems will be synthesized in the future. Seeber et al.[98] synthesized a cluster compound, $[Cl(CuCl_2tachH)_3]X_2$ (tach = *cis*,*trans*-1,3,5-triaminocyclohexane), which has the triangle cluster {Cu_3Cl} liked in the 1D chain, namely, the triangular tube (see I of Figure 3). The magnetic susceptibility data analyzed using the Heisenberg model indicated that the intrachain J value for the triangle is -9.2 K, while the intertriangle coupling is -2.7 K. Therefore, this compound exhibited a combination of spin frustration and spin chain behavior. Adachi et al.[99] reported a synthesis of two-dimensional coordination polymers $[M_8tdpd](H_2O)_2]_n$ (M = Mn(II) or Co(II)) involving a triangular lattice. The χT plots of the polymers indicated weak antiferromagnetic interactions ($J < -1.8$ K) between magnetic ions. However, no further characterization was reported.

In past decades, kagome lattices have received theoretical interest in relation to resonating VB (RVB) and spin liquid states. Helton et al.[100,101] performed thermodynamic and neutron scattering measurements on $ZnCu_3(OH)_6Cl_2$ with the $S = 1/2$ kagome lattice. Neutron diffraction experiments clearly demonstrated the absence of long-range magnetic order down to 1.8 K, though the magnetic susceptibility experiments showed the high Curie−Weiss temperature of 300 K and strong antiferromagnetic interaction of $J = -17/2$ meV (-68.5 cm^{-1}). These results are compatible with the spin liquid state and/or the RVB state. Matan et al.[102] performed a high-resolution neutron scattering study on a single crystal of iron jarosite $KFe_3(OH)_6(SO_4)_2$ with the kagome lattice constructed of Fe(III) ions ($S = 5/2$). Iron jarosites showed classical (triangular) spin alignment (broken symmetry with Neel temperature = 70 K). The transition to long-range antiferromagnetic order was ascribed to the Dzyaloshinsky−Moriya (DM) interaction; note that the magnitude of the DM term is parallel to the square of the size of the spin (S^2). Valldor et al.[103] performed the diffuse polarized neutron scattering experiments on the cobaltite Swedenborgite structure, $ABaCo_3BO_7$ (A = Y, Ca and B = Co, Fe, Al, Zn) and revealed the two-dimensional (2D) spin correlation on the kagome sublattices toward the entropically favored $\sqrt{3} \times \sqrt{3}$ structure. Zheng et al.[104] have reported a 2D compound $[Co_3(\mu_3\text{-}OH)_2(1,2\text{-chdc})_2]$ (1,2-chdc = *trans*-1,2-cyclohexane dicarboxylate) comprising triangular arrays of $Co_3(\mu_3\text{-}OH)_2$ which afford a Kagome-like lattice. The χT plot of this material indicated the coexistence of spin frustration and long-range magnetic ordering. Manson et al.[105] synthesized three-dimensional coordination network solids of M(II)[C-(CN)$_3$]$_2$ (M = Cr, V) with a triangular array of the M(II) ions, akin to a kagome lattice. The Curie−Weiss plot for these materials indicated negative (antiferromagnetic) Weiss temperature ($\Theta = -67$ and -46 K for V and Cr ions, respectively). Long-range magnetic order did not occur for M = V(II) above 1.7 K, in contrast to that for M = Cr(II), which antiferromagnetically ordered at a low temperature. The reported experimental results[97−107] indicated that spin frustration effects are highly dependent on the size of component spins even if triangle and kagome lattices are constructed.

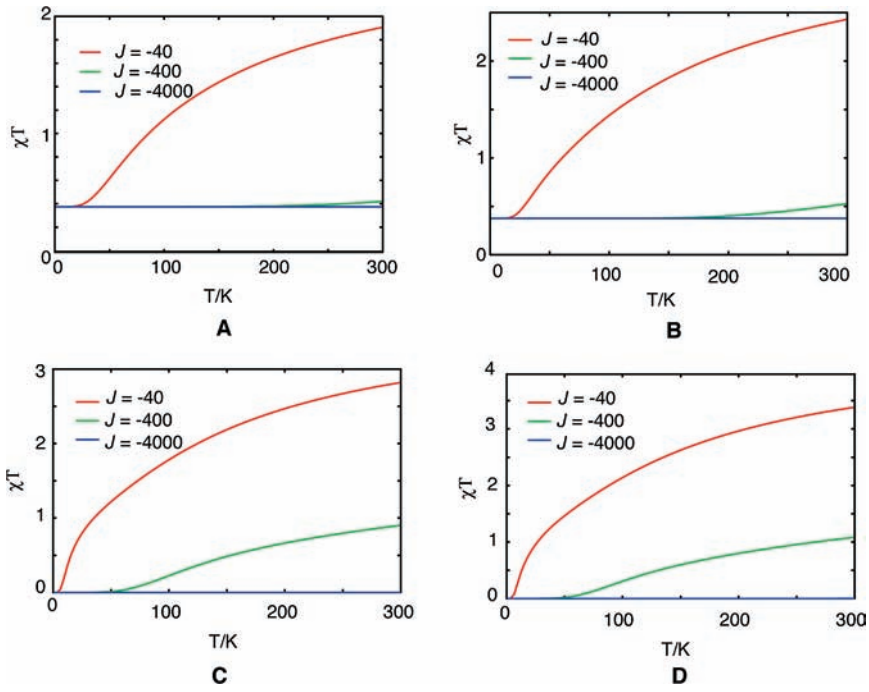

Figure 15. Magnetic susceptibilities for the cluster models (A−D) calculated with the energy levels in Figure 14 assuming effective exchange integrals; $J = -40$ (weak), -400 (intermediate), and -4000 (strong) (cm^{-1}). The magnetic susceptibility in the range of $T < 300$ K was constant for (A) and (B) and zero for (C) and (D) for the $J = -4000$ cm^{-1} case. The magnetic susceptibility for (C) and (D) was developed in the higher-temperature region ($T > 100$ K) for the case with $J = -400$ cm^{-1}. On the other hand, the magnetic susceptibility exhibited typical antiferromagnetic behavior for the $J = -40$ cm^{-1} case.

IV.3. Crossover between Classical and Quantum Spins. Self-organization is one of key concepts in bottom-up synthesis of molecule-based materials. Weak interactions such as hydrogen bonding, van der Waals interaction, and coordination bonding play an important role on the construction of such well-organized systems, though rational design of component molecules is crucial. For example, self-organization of transition-metal complexes with appropriate ligands (L) may provide Archimedes quasi-polyhedrons with $(M)_x(L)_y$ structures (number of transition-metal ions (M): $x = 6$, 12, 24, 30, and 60) Such molecule-based spin clusters with geometrical frustration are interesting targets to investigate the crossover from the quantum to classical nature of spin since the size of the spin site (S) may be controlled with chemical design. Anderson discussed the resonant frequency $\omega = J/hN$ for recovery of spin symmetry via resonance of clusters spins.[121] The ω value for quantum resonance is essentially zero if the number of state N exceeds a certain limit, indicating a possibility of symmetry breaking. Muller and his collaborators have synthesized Keplerrate structural-type magnetic molecules abbreviated as $Mo_{72}M_{30}$, which has a highly symmetric array of 30 exchange-coupled magnetic ions M^{m+} in an icosidodecahedron cluster, a closed spherical structure consisting of 20 corner-sharing triangles arranged around 12 pentagones. The magnetic ions M^{m+} are Fe(III) with $S = 5/2$, Cr(III) with $S = 3/2$, and V(IV) with $S = 1/2$.[110−120] The observed J value between Fe(III) ions was -0.8 K, showing weak antiferromagnetic exchange interaction, while the corresponding interactions for V(IV) ions was found to be relatively strong ($J = -125$ K). The numbers of the spin state $(2S + 1)^N$ are variable as follows: $(6)^{30} = 10^{22}$ for $Fe(III)_{30}$, $(4)^{30} = 10^{18}$ for $Cr(III)_{30}$, and $(2)^{30} = 10^9$ for $V(IV)_{30}$, respectively. The number of the spin state for $Fe(III)_{30}$ is close to the thermodynamic limit, but it is smaller than 10^{10} for $V(IV)_{30}$. This suggests that the spin $S = 5/2$ on Fe(III) is essentially regarded as classical, but the spin=1/2 on V(IV) is purely quantum. In fact, several experimental observations have shown that spins of the $Fe(III)_{30}$ cluster are freezing like in single-molecule magnets, compatible with classical spin, and spins of the $V(IV)_{30}$ cluster exhibit the singlet pairing in accord with the resonating VB (RVB) state. The magnetic behavior of spins of the $Cr(III)_{30}$ cluster is rather similar to that of the $Fe(III)_{30}$ cluster, showing the classical nature at finite temperature.

Yamanaka et al. have performed the GSO DFT computations of the model cluster (H_{30}) assuming the geometry of $Mo_{72}Fe_{30}$.[122] The total energies of three different BS DFT solutions arising from the magnetic double group theory indicated the following stability order: $E(M(e)) < E(GIh) < E(GHS)$, where M(e) means the helical SDW (HSDW) solution with 20 triangles on the spherical surface of the icosidodecahedron (Ih) polyhedron, while GIh and GHS denote the noncollinear GSO and high-spin-type solutions with Ih magnetic symmetry, respectively. The greater stability of E(M(e)) than E(GHS) clearly indicated the antiferromagnetic interaction (calculated $J = -13.7$ cm^{-1}), in accord with the experimental trends. The HSDW solution is approximated with the classical Heisenberg model as

$$E(\mathrm{HSDW})_{30} = 20E(\mathrm{HSDW})_3 = 60JS(S+1) \quad (27a)$$

where the HSDW solution has 30 spins that are decomposed into 20 triangles. On the other hand, the HSDW after quantum correction is given by

$$\begin{aligned} \langle H\rangle_0 &= \langle \sum_{i=1}^{20} H_{20}\rangle_0 \geq \sum_{i=1}^{20} \langle H_3\rangle_0 \\ &= \sum_{i=1}^{20} [-J\{\langle (\mathbf{S}_1 + \mathbf{S}_2 + \mathbf{S}_3)^2\rangle - 3S(S+1)\}] \\ &= 60J\{S(S+1) - 3/4\} \end{aligned} \quad (27b)$$

Thus, classical and quantum Heisenberg models supported triangle (GSO) and resonating GSO (triangle) pictures even in the Ih cluster instead of collinear and resonating collinear pictures. However, the Dzyaloshinski−Moriya (DM) interaction

may become important for further characterization of the spin states of the *Ih* clusters. The GSO DFT computations of true M_{30} clusters including spin−orbit interactions are interesting future problems.

IV.4. Hyperkagome Systems. Very recently, Takagi and his collaborators[123] have discovered a new class of spin frustration systems, $Na_4Ir_3O_8$. It has the so-called pyrocholre lattice, a network of corner-shared tetrahedrra, where each tetrahedron is occupied by three Ir and one Na, giving rise to a network of corner-shared Ir triangles called a hyperkagome lattice, namely, a three-dimensional (3D) spin frustrated system. Ir in this compound is tetravalent with five 5d electrons in the octahedron coordination, indicating a low-spin ($S = 1/2$) (t_{2g}^5) state. The temperature-dependent magnetic susceptibility demonstrated that $Na_4Ir_3O_8$ is a frustrated $S = 1/2$ system with a strong antiferromagnetic interaction with the Curie−Weiss (CW) constant $\theta = -650$ K. The geometrical frustration in this hyperkagome lattice was extremely strong, indicating no long-range order in the susceptibility even down to 2 K, which is 2 orders of magnitude lower than CW temperature. The neutron diffraction measurement at 10 K did not indicate any signature of ordering. The specific heat data showed a broad peak with its maximum at around 30 K but no anomaly indicative of long-range ordering. These experimental results are consistent with a spin liquid ground state in $Na_4Ir_3O_8$.

Theoretical studies have been initiated assuming both classical and quantum Heisenberg models using several methods, (a) exact diagonalization, (b) Monte Calro simulation, (c) cluster dynamical mean field theory, (d) field-theoretical analysis with Gutzwiller projection, and (e) others such as large-*N* mean field theory.[124−131] Monte Carlo simulation of the classical spin model indicated that a nematic order emerges at low temperature via order by disorder, representing the dominance of coplanar spin configurations. Theoretical investigation[126,127] based quantum spin models have revealed several possible quantum states of the hyperkagome systems, (1) U(1)-uniform state, (2) U(1)-staggred state, (3) Z2 state, and (4) chiral states. The transition at 20 K has been interpreted as a transition between a U(1) spin liquid and a Z2 spin liquid, where spinons are paired at low temperature.[128] On the other hand, a cluster dynamical mean field calculation[131] including both spin and charge fluctuations within the Hubbard model indicated the pseudogap-like feature and two singularities, the van-Hove singularity and the flat band in the metallic regime. Therefore, the Mott transition between insulating and metallic regimes in hyperkagome lattices is interesting, leading to importance of chemical syntheses of hyperkagome compounds for further experimental investigations. Since relative stabilities among several phases are sensitive to sign and magnitude of *J* values and DM parameters via spin−orbit interaction, ab initio calculations of them are also important for molecular design of such exotic materials.

V. Concluding Remarks

After the discovery of high-T_c superconductivity,[132] we performed molecular design of isoelectronic systems to copper−oxygen bonds to form zero- and low-dimensional networks of spins assuming magnetic mechanisms such as magnetic excitation and spin frustration instead of the singlet exciton model.[87] Several two-center three-electron bonds (X−Y) like the Cu(II)−O bond have been examined to construct such spin networks with second- and third-row non-transition-metal elements.[88−90] Recently, several groups have discovered triangular systems with spin frustration. For example, the Saito−Kanoda group[23] performed ^{1}H NMR and static magnetic susceptibility measurements on an organic Mott insulator with a nearly isotropic triangular lattice, κ-(BEDT-TTF)$_2$Cu$_2$(CN)$_3$, which is a model system of frustrated quantum spins. The ^{1}H NMR spectra showed no indication of long-range magnetic ordering down to 32 mK, which is 4 orders of magnitude smaller than the magnitude of the effective exchange constant $J = -250/2$ K found with the magnetic susceptibility measurements. Their results indicated that a quantum spin liquid state is realized in the close proximity of the superconducting state appearing under pressure. Kawakami et al.[133] have already performed the HDFT computations of *J* values and exact diagonalization of the resulting Heisenberg Hamiltonian for κ-(BEDT-TTF)$_2$Cu$_2$(CN)$_3$. They[134] have also conducted similar studies on β'-Me$_4$P[Pd(dmit)$_2$]$_2$.[22]

Self-organization by the use of weak interaction is a guiding principle for construction of molecule-based materials such as κ-(BEDT-TTF)$_2$Cu$_2$(CN)$_3$. Then, the intermolecular interactions such as $|J|$ are not so strong, giving rise to a low transition temperature. On the other hand, present computations showed that much larger $|J|$ values are possible for chemical bonding (X−Y) systems, as shown in Figures 3−8. Physical chemistry techniques using extreme conditions such as high external fields (temperature, pressure, electronic field, magnetic field, etc.) might be useful for constructions of exotic materials with spin networks discussed in this paper; note that stable compounds such as C_{60} have been synthesized, but stabilization of exchange-forbidden transition state (see Schemes 3 and 4), namely, the spin triangle, with the formation of networks was not realized yet in the case of 2p and 3p electron systems. Bottom-up syntheses of spin network systems are interesting and important not only from the viewpoint of basic spin science but also for future applications to molecular spin devices. Quantum simulation techniques starting from ab initio computations of magnetic interaction parameters (*J*, *D*, *E*, and so on) are shown to be useful for rational design of spin frustation systems.

Acknowledgment. One of the authors (K.Y.) thanks Professor Vincenzo Aquilanti and Professor Toshio Kasai for kind discussions of symmetry breaking in molecular science and bottom-up syntheses of new materials with molecular beam techniques by the use of external electronic and magnetic fields. The authors thank Professor Katsuya Inoue for kind discussions of chiral spin structure. This work was supported by Grants-in-Aid for Scientific Research (Nos. 19750005, 18205023, and 18350008) from the Japan Society for the promotion of Science (JSPS).

Supporting Information Available: Supporting materials are available for lucid understanding of basic concepts and necessary mathematical formulations for spin frustrated systems. Supporting figures (S1−S10) and Tables S1−S3 are also given for theoretical explanations of the spin frustrated systems. This material is available free of charge via the Internet at http://pubs.acs.org.

References and Notes

(1) Husimi, K.; Syozi, I. *Prog. Theor. Phys.* **1950**, *5*, 177.
(2) Syozi, I. *Prog. Theor. Phys.* **1950**, *5*, 341.
(3) Wannier, G. H. *Phys. Rev.* **1950**, *79*, 367.
(4) Yoshimori, A. *J. Phys. Soc. Jpn.* **1959**, *14*, 807.
(5) Villain, J. *J. Phys. Chem. Solids.* **1959**, *11*, 303.
(6) Kaplan, T. A. *Phys. Rev.* **1959**, *116*, 888.
(7) Kosterlitz, J. M.; Thouless, D. J. *J. Phys. C* **1973**, *6*, 1181.
(8) Anderson, P. W. *Mater. Res. Bull.* **1973**, *8*, 153.
(9) Fazekas, P.; Anderson, P. W. *Philos. Mag.* **1974**, *30*, 423.
(10) Toulouse, G. *Commun. Phys.* **1977**, *2*, 115.
(11) Vannimenus, J.; Toulouse, G. *J. Phys. C* **1977**, *10*, L537.

(12) Kawamura, H.; Miyashita, S. *J. Phys. Soc. Jpn.* **1984**, *53*, 9.
(13) Miyashita, S.; Shiba, H. *J. Phys. Soc. Jpn.* **1984**, *53*, 1145.
(14) Anderson, P. W. *Science* **1987**, *235*, 1196.
(15) Jolicoeur, T.; Le Guillou, J. C. *Phys. Rev. B* **1989**, *40*, 2727.
(16) Goto, T.; Inami, T.; Ajiro, Y. *J. Phys. Soc. Jpn.* **1990**, *59*, 2328.
(17) Awaga, K.; et al. *Chem. Phys. Lett.* **1992**, *195*, 21.
(18) Bernu, B.; Lecheminant, P.; Lhuillier, C.; Pierre, L. *Phys. Rev. B* **1994**, *50*, 10048.
(19) Lee, S. H.; Broholm, C.; Aeppli, G.; Perring, T. G.; Hessen, B.; Taylor, A. *Phys. Rev. Lett.* **1996**, *76*, 4424.
(20) Lecheminant, P.; Bernu, B.; Lhuillier, C.; Pierre, L.; Sindzingre, P. *Phys. Rev. B* **1997**, *56*, 2521.
(21) Capriotti, L.; Trumper, A.; Sorella, S. *Phys. Rev. Lett.* **1999**, *82*, 3899.
(22) Tamura, M.; Kato, R. *J. Phys.: Condens. Matter* **2002**, *14*, L729.
(23) Shimizu, Y.; Miyagawa, K.; Kanoda, K.; Maesato, M.; Saito, G. *Phys. Rev. Lett.* **2003**, *91*, 107001.
(24) Motrunick, O. I. *Phys. Rev. B* **2005**, *72*, 045105.
(25) Lee, S.-S.; Lee, P. A *Phys. Rev. Lett.* **2005**, *95*, 036403.
(26) Anderson, P. W. *Phys. Rev. Lett.* **2006**, *96*, 017001.
(27) Shores, M. P.; Nytko, E. A.; Bartlett, B. M.; Nocera, D. G. *J. Am. Chem. Soc.* **2007**, *127*, 13462.
(28) Ryu, S.; Motrunick, O. I.; Alicea, J.; Fisher, M. P. A. *Phys. Rev. B* **2007**, *75*, 184406.
(29) Castelnoro, C.; Moessner, R.; Sondhi, S. L. *Nature* **2008**, *451*, 42.
(30) Heiler, W.; London, F. *Z. Phys.* **1927**, *44*, 455.
(31) Slater, J. C. *Phys. Rev.* **1931**, *38*, 1109.
(32) Pauling, L. *J. Am. Chem. Soc.* **1931**, *53*, 1367.
(33) Yamaguchi, K. *Chem. Phys. Lett.* **1975**, *30*, 288.
(34) Yamaguchi, K. *Chem. Phys. Lett.* **1975**, *34*, 434.
(35) Yamaguchi, K. *Chem. Phys. Lett.* **1974**, *28*, 93.
(36) London, F. *Z. Electrochem.* **1929**, *35*, 552.
(37) Eyring, H.; Polanyi, M. *Z. Phys. Chem. B* **1931**, *12*, 279.
(38) Glasstone, S.; Laidler, K. J.; Eyring, H. *The Theory of Rate Processes*; McGraw-Hill: New York, 1941.
(39) Wheland, G. W. *The Theory of Resonance*; John Wiley: New York, 1944.
(40) Yamaguchi, K.; Takahara, Y.; Fueno, T. In *Applied Quantum Chemistry*; Smith, V. H., Jr., Scheafer, H. F., III, Morokuma, K., Eds; Reidel D.: Boston, MA, 1986; p 155.
(41) Yamaguchi, K. In *Singlet Oxygen*; Frimer, A. A., Ed.; CRC Press: Boca Raton, FL, 1985; Vol. III, p 237.
(42) Yamaguchi, K.; Takahara, Y.; Fueno, T. In *The Role of Oxygen in Chemistry and Biology*; Ando, W., Moro-oka, Y., Eds.; Elsevier: Amsterdam, The Netherlands, 1988; p 263.
(43) Harris, D. L.; Loew, G. H. *J. Am. Chem. Soc.* **1998**, *120*, 8941.
(44) Shaik, S.; Filatov, M.; Schroder, D.; Schwarz, H. *Chem.—Eur. J.* **1998**, *4*, 193.
(45) Ogliaro, F.; Harris, N.; Cohen, S.; Filatov, M.; de Visser, S. P.; Shaik, S. *J. Am. Chem. Soc.* **2000**, *122*, 8977.
(46) Ogliaro, F.; Cohen, S.; de Visser, S. P.; Shaik, S. *J. Am. Chem. Soc.* **2000**, *122*, 12892.
(47) Ogliaro, F.; de Visser, S. P.; Cohen, S.; Sharma, P. K.; Shaik, S. *J. Am. Chem. Soc.* **2002**, *124*, 2806.
(48) Schöneboom, J. C.; Cohen, S.; Lin, H.; Shaik, S.; Thiel, W. *J. Am. Chem. Soc.* **2004**, *126*, 4017.
(49) Altun, A.; Shaik, S.; Thiel, W. *J. Am. Chem. Soc.* **2007**, *129*, 8978.
(50) Yoshizawa, K.; Shiota, Y.; Kagawa, Y. *Bull. Chem. Soc. Jpn.* **2000**, *73*, 2669.
(51) Yoshizawa, K. *J. Organomet. Chem.* **2001**, *635*, 100.
(52) Kamachi, T.; Yoshizawa, K. *J. Am. Chem. Soc.* **2003**, *125*, 4652.
(53) Gaullar, V.; Friesner, R. A. *J. Am. Chem. Soc.* **2004**, *126*, 8501.
(54) Jovanovic, T.; Farid, R.; Friesner, R. A.; McDermott, A. E. *J. Am. Chem. Soc.* **2005**, *127*, 13548.
(55) Ravindranatharn, K. P.; Gallicchio, E.; Friesner, R. A.; McDermott, A. E.; Levy, R. M. *J. Am. Chem. Soc.* **2006**, *128*, 5786.
(56) Bach, R. D.; Dmitrenko, O. *J. Am. Chem. Soc.* **2006**, *128*, 1474.
(57) Shoji, M.; Isobe, H.; Takano, Y.; Kitagawa, Y.; Yamanaka, S.; Okumura, M.; Yamaguchi, K. *Int. J. Quantum Chem.* **2007**, *108*, 3250.
(58) Shoji, M.; Isobe, H.; Saito, T.; Yabushita, H.; Koizumi, K.; Kitagawa, Y.; Yamanaka, S.; Kawakami, T.; Okumura, M.; Hagiwara, M.; Yamaguchi, K. *Int. J. Quantum Chem.* **2008**, *108*, 631.
(59) Shoji, M.; et al. *Int. J. Quantum Chem.* **2008**, *107*, 3250.
(60) Isobe, H.; Nishihara, S.; Shoji, M.; Yamanaka, S.; Shimada, J.; Hagiwara, M.; Yamaguchi, K. *Int. J. Quantum Chem.* **2008**, *108*, 2991.
(61) Yamaguchi, K. *Int. J. Quantum Chem.* **1980**, *S14*, 269.
(62) Yamaguchi, K. *J. Mol. Struct.: THEOCHEM* **1983**, *103*, 101, part I of this series.
(63) Yamaguchi, K.; Yamanaka, S.; Nishino, M.; Takano, Y.; Kitagawa, Y.; Nagao, H.; Yoshioka, Y. *Theor. Chem. Acc.* **1999**, *102*, 328, part II of this series.
(64) Fund, F. *Z. Phys.* **1927**, *40*, 742.
(65) Mulliken, R. S. *Phys. Rev.* **1932**, *41*, 49.
(66) Yamaguchi, K. *Self Consistent Field: Theory and Applications*; Carbo, R., Klobowsky, M., Eds.; Elsevier: New York, 1990; p 727
(67) Yamaguchi, K. *Chem. Phys. Lett.* **1975**, *33*, 330.
(68) Yamaguchi, K. *Chem. Phys. Lett.* **1975**, *35*, 230.
(69) Yamaguchi, K. *Chem. Phys. Lett.* **1979**, *68*, 477.
(70) Yamaguchi, K.; Fueno, T.; Fukutome, H. *Chem. Phys. Lett.* **1973**, *22*, 461.
(71) Yamaguchi, K.; Fueno, T. *Chem. Phys.* **1977**, *19*, 35.
(72) Yamaguchi, K.; Fueno, T. *Chem. Phys.* **1977**, *23*, 375.
(73) Weinbaum, S. *J. Chem. Phys.* **1933**, *1*, 593.
(74) Hubbard, J. *Proc. R. Soc. London, Ser. A* **1958**, *244*, 199.
(75) Yamaguchi, K.; Kawakami, T.; Takano, Y.; Kitagawa, Y.; Yamashita, Y.; Fujita, H. *Int. J. Quantum Chem.* **2002**, *90*, 370.
(76) Nishirara, S.; Yamanaka, S.; Nakata, K.; Kitagawa, Y.; Yonezawa, Y.; Okumura, M.; Nakamura, H.; Takada, T.; Yamaguchi, K. *Polyhedron* **2009**, *28*, 1628.
(77) Yamaguchi, K.; Yoshioka, Y.; Takatsuka, K.; Fueno, T. *Theoret. Chim. Acta.* **1978**, *48*, 185.
(78) Kubo, K.; Momoi, T. *Z. Phys. B: Condens. Matter* **1997**, *103*, 485.
(79) Misguich, G.; Lhuillier, C.; Bernu, B.; Waldmann, C. *Phys. Rev. B* **1999**, *60*, 1064.
(80) Yamanaka, S.; Yamaki, D.; Takeda, R.; Nagao, H.; Yamaguchi, K. *Int. J. Quantum Chem.* **2004**, *100*, 1179.
(81) Yamanaka, S.; Takeda, R.; Shoji, M.; Koizumi, K.; Kitagawa, Y.; Yamaguchi, K. *Polyhedron* **2005**, *24*, 2784.
(82) Yamaki, D.; Shigeta, Y.; Yamanaka, S.; Nagao, H.; Yamaguchi, K. *Int. J. Quantum Chem.* **2000**, *80*, 701.
(83) Yamanaka, S.; Shigeta, Y.; Ohta, Y.; Yamaki, D.; Nagao, H.; Yamaguchi, K. *Int. J. Quantum Chem.* **2001**, *84*, 369.
(84) Tadeda, R.; Yamanaka, S.; Yamaguchi, K. *Int. J. Quantum Chem.* **2006**, *106*, 3303.
(85) Tadeda, R.; Yamanaka, S.; Yamaguchi, K. *Int. J. Quantum Chem.* **2007**, *107*, 2317.
(86) Nishihara, S.; Yamanaka, S.; Kusakabe, K.; Nakata, K.; Yonezawa, Y.; Nakamura, H.; Takada, T.; Yamaguchi, K. *J. Phys.: Condens. Matter.* **2009**, *21*, 064227.
(87) Little, W. A. *Phys. Rev.* **1964**, *134*, 1416.
(88) Yamaguchi, K.; Takahara, Y.; Feuno, T.; Nakasuji, K.; Murata, I. *Jpn. J. Appl. Phys.* **1988**, *27*, 766.
(89) Yamaguchi, K.; Yamaki, D.; Kitagawa, Y.; Takahata, M.; Kawakami, T.; Ohsaku, T.; Nagao, H. *Int. J. Quantum Chem.* **2003**, *92*, 47.
(90) Yamaguchi, K. *Int. J. Quantum Chem.* **1990**, *37*, 167.
(91) Yamaguchi, K.; Nakano, M.; Nagao, H.; Okumura, M.; Yamanaka, S.; Kawakami, T.; Yamada, S.; Yamaki, D.; Kitagawa, Y.; Takeda, R.; Nitta, H. *Int. J. Quantum Chem.* **2006**, *106*, 1052.
(92) Mitani, M.; Mori, H.; Takano, Y.; Yamaki, D.; Yoshioka, Y.; Yamaguchi, K. *J. Chem. Phys.* **2000**, *113*, 4035.
(93) Mitani, M.; Yamaki, D.; Takano, Y.; Kitagawa, Y.; Yoshioka, Y.; Yamaguchi, K. *J. Chem. Phys.* **2000**, *113*, 10486.
(94) Choi, K.-Y.; Matsuda, Y. H.; Nojiri, H.; Kortz, U.; Hussain, F.; Stowe, A. C.; Ramsey, C.; Dalal, N. S. *Phys. Rev. Lett.* **2006**, *96*, 107202.
(95) Choi, K. Y.; Dalal, N. S.; Reyes, A. P.; Kuhns, P. L.; Matsuda, Y. H.; Nojiri, H.; Mal, S. S.; Kortz, U. *Phys. Rev. B* **2008**, *77*, 024406.
(96) Yoneda, K.; Adachi, K.; Nishio, K.; Yamasaki, M.; Fuyuhiro, A.; Katada, M.; Kaizaki, S.; Kawata, S. *Angew. Chem., Int. Ed.* **2006**, *45*, 5459.
(97) Cador, O.; Gatteschi, D.; Sessoli, R.; Barra, A.-L.; Timco, G. A.; Winpenny, R. E. P. *J. Magn. Magn. Mater.* **2005**, *290−291*, 55.
(98) Seeber, G.; Kogerler, P.; Kariuki, B. M.; Cronin, L. *Chem. Commun.* 2004.
(99) Adachi, K.; Kawata, S.; Kabir, M. K.; Kumagai, H.; Inoue, K.; Kitagawa, S. *Chem. Lett.* **2001**, 50.
(100) Shores, M. P.; Mytko, E. A.; Bartlett, B. M.; Nocera, D. G. *J. Am. Chem. Soc.* **2005**, *127*, 13462.
(101) Helton, J. S.; Matan, K.; Shores, M. P.; Nytko, E. A.; Bartlett, B. M.; Yoshida, Y.; Takano, Y.; Suslov, A.; Oiu, Y.; Chung, J.-H.; Lee, Y. S. *Phys. Rev. Lett.* **2007**, *98*, 107204.
(102) Matan, K.; Grohol, D.; Nocera, D. G.; Yildirim, T.; Harris, A. B.; Lee, S. H.; Nagler, S. E.; Lee, Y. S. *Phys. Rev. Lett.* **2006**, *96*, 247201.
(103) Valldor, M.; Sanders, Y.; Schweika, W. *J. Phys. Conf. Ser.* **2009**, *145*, 012076.
(104) Zheng, Y.-Z.; Tong, M.-L.; Zhang, W.-X; Chen, X.-M. *Chem. Commun.* **2006**, 165.
(105) Manson, J. L.; Ressouche, E.; Miller, J. S. *Inorg. Chem.* **2000**, *39*, 1135.
(106) Zhang, X.-M.; Jiang, T.; Wu, H.-S.; Zeng, M.-H *Inorg. Chem.* **2009**, *48*, 4536.
(107) Yamaguchi, K.; Fueno, T.; Ozaki, M.; Ueyama, N.; Nakamura, A. *Chem. Phys. Lett.* **1990**, *168*, 56.
(108) Yamanaka, S.; Takeda, R.; Yamaguchi, K. *J. Magn. Magn. Mater.* **2004**, *272−276*, e255.

(109) Yamanaka, S.; Takeda, R.; Yamaguchi, K. *Polyhedron* **2003**, *22*, 2013.

(110) Muller, A.; Sarkar, S.; Shah, S. O. N.; Bogge, H.; Schmidtmann, M.; Sarkar, S.; Kogerler, P.; Hauptfleisch, B.; Trautwein, A. X.; Schnemann, V. *Angew. Chem., Int. Ed.* **1999**, *38*, 3238.

(111) Muller, A.; Luban, M.; Schoder, C.; Modler, R.; Kogerler, P.; Axenovich, M.; Schnack, J.; Canfield, P.; Budko, S.; Harrison, N. *Chem. Phys. Chem.* **2001**, *2*, 517.

(112) Muller, A.; Todea, A. M.; von Slageren, J.; Dressel, M.; Bogge, H.; Schmidmann, M.; Luban, M.; Englehardt, L.; Rusu, M. *Angew. Chem., Int. Ed.* **2005**, *44*, 3857.

(113) Schroder, C.; Nojiri, H.; Scnack, J.; Hage, P.; Luban, M.; Kogerler, K. *Phys. Rev. Lett.* **2005**, *94*, 017205.

(114) Schnack, J.; Luban, M.; Modler, R. *Europhys. Lett.* **2001**, *56*, 863.

(115) Botar, B.; Kogerler, P.; Hill, C. L. *Chem. Commun.* **2005**, 3138.

(116) Kunisada, N.; Takemura, S.; Fukumoto, Y. *J. Phys. Conf. Ser.* **2009**, *145*, 012083.

(117) Schroder; Prozorov, R.; Kogerler, P.; Vannette, M. D.; Fang, X.; Luban, M.; Matsuo, A.; Kindo, K.; Muller, A.; Toeda, A. M. *Phys. Rev. B* **2008**, *77*, 224409.

(118) Garlea, V. O.; Nagler, S. E.; Zarestky, J. L.; Stassis, C.; Vaknin, D.; Kogerler, P.; McMorrow, D. F.; Niedermayer, C.; Tennant, D. A.; Lake, B.; Qiu, Y.; Exler, M.; Schnack, J.; Luban, M. *Phys. Rev. B* **2006**, *73*, 024414.

(119) Schroder, C.; Schnack, J.; Mentrup, D.; Luban, M. *J. Magn. Magn. Mater.* **2004**, *272*−*276*, e721.

(120) Tarantul, A.; Tsukerblat, B.; Muller, A. *Solid State Sci.* **2008**, *10*, 1814.

(121) Anderson, P. W. *Phys. Rev.* **l952**, *86*, 694.

(122) Yamanaka, S.; Takeda, R.; Yamaguchi, K. *Int. J. Quantum Chem.* **2004**, *102*, 334.

(123) Okamoto, Y.; Nohara, M.; Aruga-Katori, H.; Tagaki, H. *Phys. Rev. Lett.* **2007**, *99*, 137207.

(124) Lee, P. A. *Science* **2008**, *321*, 1306.

(125) Hopkinson, J. M.; Isakov, S. V.; Kee, H.-Y.; Kim, Y. B. *Phys. Rev. Lett.* **2007**, *99*, 037201.

(126) Lawler, M. J.; Kee, H.-Y.; Kim, Y. B.; Vishwanath, A. *Phys. Rev. Lett.* **2008**, *100*, 227201.

(127) Lawler, M. J.; Paramekanti, A.; Kim, Y. B.; Balents, L. *Phys. Rev. Lett.* **2008**, *101*, 197202.

(128) Zhou, Y.; Lee, P. A.; Ng, T.-K.; Zhang, F.-C. *Phys. Rev. Lett.* **2008**, *101*, 197201.

(129) Chen, G.; Balents, L. *Phys. Rev. B* **2008**, *78*, 094403.

(130) Zhitomirsky, M. E. *Phys. Rev. B* **2008**, *78*, 094423.

(131) Udagawa, M.; Motome, Y. *J. Phys. Conf. Ser.* **2009**, *145*, 012013.

(132) Bednort, J. G.; Muller, K. A. *Z. Phys.* **1986**, *64*, 189.

(133) Kawakami, T.; Taniguchi, T.; Shoji, M.; Kitagawa, Y.; Yamanaka, S.; Okumura, M.; Yamaguchi, K. *Mol. Cryst. Liq. Cryst.* **2006**, *455*, 133.

(134) Kawakami, T.; Shoji, M.; Taniguchi, T.; Nishimura, Y.; Takenaka, M.; Kitagawa, Y.; Yamanaka, S.; Okumura, M.; Yamaguchi, K. In *The Proceeding of the Symposium Science and Engineering of the Future with Multifunctional Conducting Molecular Materials*; Saito, G. et al., Eds., RSC Pub.: London, 2007; p 101.

JP905991R